Tris-chelated complexes of nickel(II) with bipyridine derivatives: DNA binding and cleavage, BSA binding, molecular docking, and cytotoxicity

Marzieh Anjomshoa, Masoud Torkzadeh-Mahani, Mehdi Sahihi, Corrado Rizzoli, Mehdi Ansari, Jan Janczak, Sheila Sherafat Esfahani, Farangis Ataei, Monireh Dehkhodaei, Bagher Amirheidari

Journal of Biomolecular Structure and Dynamics

Tris-chelated complexes of nickel(II) with bipyridine derivatives: DNA binding and cleavage, BSA binding, molecular docking, and cytotoxicity

Marzieh Anjomshoa [a], Masoud Torkzadeh-Mahani [b], Mehdi Sahihi [c], Corrado Rizzoli [d], Mehdi Ansari [a], Jan Janczak [e], Sheila Sherafat Esfahani [b], Farangis Ataei[f], Monireh Dehkhodaei[c], Bagher Amirheidari [a,*],

[a]Pharmaceutics Research Center, Institute of Neuropharmacology, Kerman University of Medical Sciences, Kerman, Iran.
[b]Department of Biotechnology, Institute of Science and High Technology and Environmental Sciences, Graduate University of Advanced Technology, Kerman, Iran.
[c]Department of Chemistry, University of Isfahan, Isfahan 81746-73441, Iran.
[d]Department of Chemistry, Life Sciences and Environmental Sustainability, University of Parma, Parco Area delle Scienze 17/A, I-43124 Parma, Italy.
[e]Institute of Low Temperature and Structure Research, Polish Academy of Sciences, P.O. Box 1410, Okólna 2 Str., 50-950 Wrocław, Poland.
[f]Department of Biochemistry, Faculty of Biological Sciences, Tarbiat Modares University, Tehran, Iran.

Number of Pages: 52
Number of Tables: 8 (+ 1 table in Supplementary material)
Number of Figures: 18 (+ 9 Figs. in Supplementary material)
Number of Schemes: 1

[*]Corresponding author,
Bagher Amirheidari
Assistant Professor of Biotechnology
Pharmaceutics Research Center, Institute of Neuropharmacology, Kerman University of Medical Sciences, Kerman, Iran.
E-mail address: **b_amirheidari@kmu.ac.ir**

Crystallographic data for the structural analysis has been deposited with the Cambridge Crystallographic Data Centre, CCDC No. 1433225 for $[Ni(dimethylbpy)_3](ClO_4)_2 \cdot 2H_2O$.

Journal of Biomolecular Structure and Dynamics

Tris-chelated complexes of nickel(II) with bipyridine derivatives: DNA binding and cleavage, BSA binding, molecular docking, and cytotoxicity

Marzieh Anjomshoa [a], Masoud Torkzadeh-Mahani [b], Mehdi Sahihi [c], Corrado Rizzoli [d], Mehdi Ansari [a], Jan Janczak [e], Sheila Sherafat Esfahani [b], Farangis Ataei[f], Monireh Dehkhodaei[c], Bagher Amirheidari [a,*],

[a]Pharmaceutics Research Center, Institute of Neuropharmacology, Kerman University of Medical Sciences, Kerman, Iran.
[b]Department of Biotechnology, Institute of Science and High Technology and Environmental Sciences, Graduate University of Advanced Technology, Kerman, Iran.
[c]Department of Chemistry, University of Isfahan, Isfahan 81746-73441, Iran.
[d]Department of Chemistry, Life Sciences and Environmental Sustainability, University of Parma, Parco Area delle Scienze 17/A, I-43124 Parma, Italy.
[e]Institute of Low Temperature and Structure Research, Polish Academy of Sciences, P.O. Box 1410, Okólna 2 Str., 50-950 Wrocław, Poland.
[f]Department of Biochemistry, Faculty of Biological Sciences, Tarbiat Modares University, Tehran, Iran.

Abstract

Two nickel(II) complexes with substituted bipyridine ligand of the type $[Ni(NN)_3](ClO_4)_2$, where NN is 4,4′-dimethyl-2,2′-bipyridine (dimethylbpy) (**1**) and 4,4′-dimethoxy-2,2′-bipyridine (dimethoxybpy) (**2**) have been synthesized, characterized, and their interaction with DNA and BSA studied by different physical methods. X-ray crystal structure of **1** shows a six-coordinate complex in a distorted octahedral geometry. DNA binding studies of **1** and **2** reveal that both complexes sit in DNA groove and then interact with neighboring nucleotides differently; **2** undergoes a partial intercalation. This is supprted by molecular docking studies, where hydrophobic interactions are aparent between **1** and DNA as compared to, hydrogen bonding, hydrophobic, and π-π interactions between **2** and DNA minor groove. Moreover, the two complexes exhibit oxidative cleavage of supercoiled plasmid DNA in the presence of hydrogen peroxide as an activator in the order of **1** > **2**. In terms of interaction with BSA, the results of spectroscopic methods and molecular docking show that **1** binds with BSA only *via* hydrophobic contacts while **2** interacts through hydrophobic and hydrogen bonding. It has been extensively demonstrated that the nature of the methyl- and methoxy-groups in ligands is a strong determinant of the bioactivity of nickel(II) complexes. This may justify the above

differences in biomolecular interactions. In addition, the *in vitro* cytotoxicity of the complexes on human carcinoma cells lines (MCF-7, HT-29, and U-87) has been examined by MTT assay. According to our observations, **1** and **2** display cytotoxicity activity against selected cell lines.

Keywords: Nickel(II) complexes; Bipyridine derivatives; Oxidative cleavage; DNA and BSA binding; Cytotoxicity

List of abbreviations:

Abbreviation	Meaning
bpy	2,2′-bipyridine
BSA	bovine serum albumin
CD	circular dichroism
CIF	crystallographic information file
dimethoxybpy	4,4′-dimethoxy-2,2′-bipyridine
dimethylbpy	4,4′-dimethyl-2,2′-bipyridine
DMF	dimethylformamide
5,6-dmp	5,6-dimethyl-1,10-phenanthroline
DMSO	dimethyl sulfoxide
dppt	5,6-diphenyl-3-(2-pyridyl)-1,2,4-triazine
dppz	dipyrido[3,2-a:2',3'-c]phenazine
dpq	dipyrido[3,2-d:2',3'-f]quinoxaline
EB	ethidium bromide
ESI-MS	electrospray ionization mass spectrometry
FS-DNA	fish sperm deoxyribonucleic acid
FDA	food and drug administration
FT-IR	fourier-transform infrared spectroscopy
GR	GelRed
MD	molecular dynamics
ORTEP	oak ridge thermal ellipsoid plot
phen	1,10-phenanthroline
phen-dione	1,10-phenanthroline-5,6-dione
PBD	protein data bank
qdppz	naptho[2,3-*a*]dipyrido[3,2-*h*:2',3'-*f*]phenazine-5,18-dione
SAR	structure–activity relationships
SFS	synchronous fluorescence spectroscopy
Tris	Tris(hydroxymethyl)-aminomethane

*Corresponding author. Tel.: +983431325855-7; fax: +983431325830; E-mail addresse: b_amirheidari@kmu.ac.ir (B. Amirheidari).

Graphical Abstract:

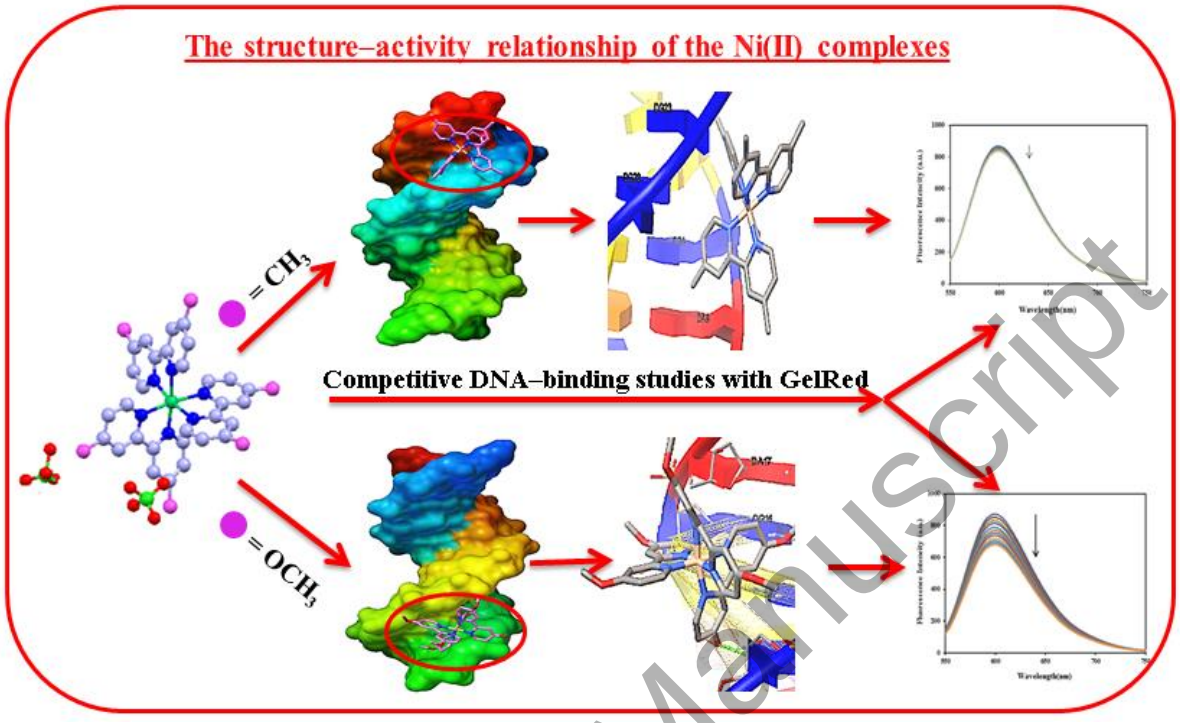

1. Introduction:

The application of transition metal complexes in antineoplastic chemotherapy has been continuously growing following the introduction of cisplatin (Rosenberg, Van Camp, Trosko, & Mansour, 1969) and its FDA approval in 1979. In spite of great success of cisplatin-like compounds, they display poor water solubility, cross resistance, and several undesirable side effects. The design and preparation of new metal based anticancer, to overcome cisplatin problems, is an attractive focus of current medicinal chemists (Rijt & Sadler, 2009). However, design criteria for such compounds are still in their initial steps; it is mainly because there is not enough understanding of structure–activity relationships (SAR) to allow providing general rules.

The ultimate target of a large percentage of chemotherapeutic drugs is DNA (Palchaudhuri & Hergenrother, 2007). The activity of this class of drugs depends on their ability to bind and induce conformational changes or damage DNA in the cancer cells, which in turn can trigger apoptosis ultimately resulting in cell death. A sensitive and easy-to-use assay for studying interaction of metal complexes with a supercoiled DNA and its cleavage is agarose gel electrophoresis, which is quite frequent in the literature (Sangeetha Gowda, Blessy Baby Mathew, Sudhamani, & Bhojya Naik, 2014). The investigation of the binding mechanism of metal complexes with serum albumins play a key role in the understanding of drug pharmacodynamics and pharmacokinetics, as the nature and strength of this interaction has a great influence on drug absorption, distribution, metabolism and excretion (Topală, Bodoki, Oprean, & Oprean, 2014). The molecular docking approach can be used to model the interaction between a metal complex and host macromolecules at the atomic level, which allow to characterize the behavior of metal complexes in the binding site of target macromolecules as well as to elucidate fundamental biochemical processes (Meng, Zhang, Mezei, & Cui, 2011). Significantly, the experimental and theoretical investigations of the

interaction and binding of metal complexes with DNA and BSA may open new avenues for the design of the most suitable drugs.

The polypyridyl complexes constitute one of the important classes of NN donors that drawn the attention of bioinorganic chemists. We have recently reported synthesis and biological activity of two copper(II) complexes with bipyridine derivatives (Anjomshoa et al., 2016). This study demonstrated aspects of the SAR of complexes in terms of the methyl- and methoxy-substituted bipyridine. Given these findings, it was desired to utilize bipyridine derivatives to make metallotherapeutic agents employing alternative metal centers. Among various metal ions, we embarked on nickel for the synthesis of complexes due to three reasons: (1) Nickel is an essential cofactor for several enzymes in many key biological processes, such as lipid metabolism and anaerobic respiration, displaying its role in determination of Ni enzyme structures and elucidation of reaction mechanisms, also implying better tolerability of nickel(II) complexes for patients (Maroney, 1999). (2) Nickle is in the same group as palladium and platinum. And, (3) nickel(II) complexes have already exhibited antimicrobial (Patra et al., 2013; Raman, Pothiraj, & Baskaran, 2011; Vinuelas-Zahinos, Luna-Giles, Torres-Garcia, & Fernandez-Calderon, 2011), antifungal (Alomar, Landreau, Allain, Bouet, & Larcher, 2013), and anticancer (Anjomshoa, Hadadzadeh, Fatemi, & Torkzadeh-Mahani, 2015; Tabrizi, Talaie, & Chiniforoshan, 2016) activities, good DNA binding affinity, and attractive DNA cleavage ability (Kosiha, Parthiban, Ciattini, Chelazzi, & Elango, 2017; Morshedi & Hadadzadeh, 2013). Arounaguiri (1996) presented the DNA-binding and photocleaving of four mixed-ligand polypyridyl nickel(II) complexes containing 1,10-phenanthroline (phen), naptho[2,3-*a*]dipyrido[3,2-*h*:2',3'-*f*]phenazine-5,18-dione (qdppz). Their report describes that substitution by different metal ions can bring about subtle modulation in the properties and, consequently, in the DNA interaction of this new class of mixed-ligand complexes containing the versatile dipyridophenazine ligand. On the other

hand, they underscore the importance of dppz in the DNA-binding among the variety of ligands utilized. Ramakrishnan and co-workers (2011) prepared a series of nickel(II) and cobalt(II) complexes, coordinated by phen, 5,6-dimethyl-1,10-phenanthroline (5,6-dmp) and dipyrido[3,2-d:2',3'-f]quinoxaline (dpq). Through investigation of the role of diimine ligands on the mode and extent of DNA binding, cleavage and anticancer effects, they demonstrated that dpq complexes show higher DNA binding affinities than phen and 5,6-dmp complexes. More interestingly, the Ni(II) complexes bond to DNA stronger than the corresponding Co(II) complexes. It is also remarkable that all of their complexes exhibited greater cytotoxicity against human breast cancer (MCF-7) cell line compared to cisplatin, wherein Ni(II) complexes were more cytotoxic than the Co(II) analogues in spite of their inability to cleave DNA. In another report, Gao (2015) reported DNA and BSA binding, DNA cleavage and cytotoxicity of a series of mononuclear mixed-ligand polypyridyl Ni(II) complexes containing a tridentate polypyridyl ligand of 4-methyl-N,N-bis(pyridin-2-ylmethyl)aniline and bpy, phen, dpq or dipyrido[3,2-a:2',3'-c]phenazine (dppz). Partial intercalation between the complexes and CT-DNA was demonstrated and binding propensity of the complexes gave the relative order of dppz > dpq > phen > bpy. They also observed that a single alteration such as the presence of glutathione (GSH) or photoirradiation at 365 nm, can drastically change the DNA cleavage abilities of complexes as compared to the absence of any external agent. Moreover, the ability of complexes to bind to BSA was also explored. In their cytotoxicity studies, dppz showed better antitumor effects and induced apoptosis in HepG-2 cells.

The above literature emphasizes on biological potential of synthesized Ni(II) complexes coordinated by different polypyridyl ligands. Accordingly, we report on the synthesis, characterization, and studying the bioactivities of new polypyridyl Ni(II) complexes of formula $[Ni(NN)_3](ClO_4)_2$, where NN is 4,4′-dimethyl-2,2′-bipyridine

(dimethylbpy) (**1**) or 4,4′-dimethoxy-2,2′-bipyridine (dimethoxybpy) (**2**) (scheme 1). The biological studies included: (i) the binding properties with fish sperm DNA (FS-DNA) by UV-visible absorption, fluorescence titration, circular dichroism (CD), (ii) the competitive DNA-binding studies with GelRed (GR) by fluorescence, (iii) the DNA cleavage activity in the absence and presence of an oxidizing agent by gel electrophoresis, (iv) the binding properties with BSA by UV-visible, emission and synchronous fluorescence spectroscopy (SFS), and CD, (v) the molecular docking and molecular dynamic simulation analyses for interaction of the complexes with DNA and BSA, and (vi) the *in vitro* cytotoxicity activity on human carcinoma cell lines (MCF-7, HT-29, and U-87) using the MTT assay for 24 and 48 h.

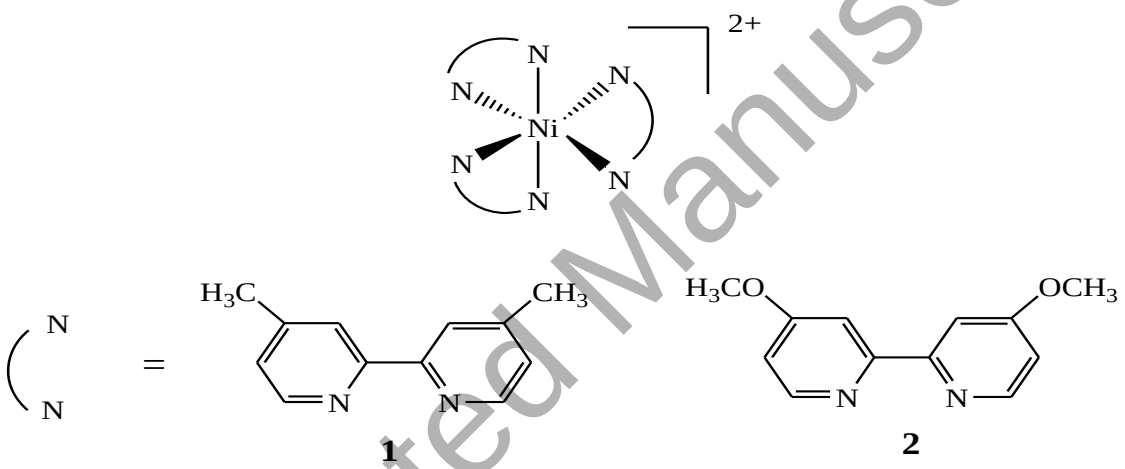

Scheme 1 Structure of the complexes and ligands used in this study.

2. Experimental Section

2.1. Materials

All chemicals, unless otherwise stated, were purchased from Sigma-Aldrich, Merck and Alfa Aesar. All materials were used as received without further purification unless noted specifically. FS-DNA was purchased from Acros, which in Tris buffer gave a A_{260}/ A_{280} ratio of 1.9, indicating it effectively free of protein (Marmur, 1961). Supercoiled pET28a DNA was extracted from an *E. coli* fresh culture by Bio Basic EZ-10 Minipreps kit. Agarose

(molecular biology grade) was purchased from Sigma-Aldrich. BSA and Tris(hydroxymethyl)-aminomethane (Tris) were purchased from Merck. Tris buffer solution, (5 mM Tris, 50 mM NaCl), was prepared using double distilled water and pH adjusted to 7.3 by titration with HCl. GelRed was purchased from Biotium. 4,4′-Dimethyl-2,2′-bipyridine and 4,4′-dimethoxy-2,2′-bipyridine were purchased from Alfa Aesar and Acros, respectively.

2.2. Instrumentation

Infrared spectra were obtained on a FT-IR Bruker-Alpha II Spectrometer. Elemental analyses were performed using a costech 4010 elemental analyzer. Electrospray ionization mass spectrometry (ESI-MS) spectra were recorded on an Agilent 6410 Triple Quadrupole LC/MS. UV-visible absorption titration was performed on a Shimadzu 3100 UV-visible spectrophotometer. Fluorescence experiments were carried out using a Varian Cary Eclipse spectrophotometer. CD spectra were recorded on an Aviv spectropolarimeter, model 215 using a cylindrical cuvette with 0.1 cm path length.

2.3. Syntheses and stability of the complexes in aqueous solution

2.3.1. Synthesis of $[Ni(dimethylbpy)_3](ClO_4)_2$ complex (1)

An ethanolic solution (10 mL) of dimethylbpy (3 mmol, 0.55 g) was added dropwise to an ethanolic solution (5 mL) of $NiCl_2.6H_2O$ (1 mmol, 0.24 g). The reaction mixture was stirred for 6 h at room temperature. The product was precipitated from solution as the perchlorate salt by adding 5 mL of a 10% aqueous solution of $NaClO_4$. The red-brown product, $[Ni(dimethylbpy)_3](ClO_4)_2$, was collected by suction filtration, washed with cold water and ether, and then air-dried. Diffusion of diethyl ether into a methanol solution of the complex gave red-brown single crystals suitable for X-ray diffraction experiments. Yield: 0.5 g, ~60%. Anal. Calc. for $C_{36}H_{40}NiN_6\ Cl_2O_{10}$ (MW = 846.35): C, 51.08; H, 4.76; N, 9.93 %.

Found: C, 51.64; H, 4.36; N, 9.77%. IR (KBr, cm^{-1}): 1617(m) ν(C=N), 1486(m) ν(C=C), and 1096(s) ν(Cl–O); ESI-MS: *m/z* 524.80 $[Ni(dimethylbpy)_2 + ClO_4]^+$, 470.9 $[Ni(bpy)_2 + ClO_4]^+$, 305.0 $[Ni(dimethylbpy)_3]^{2+}$; UV-visible λ_{max} / nm ($\varepsilon_{max} \times 10^3/M^{-1}\ cm^{-1}$): 231 (28), 249 (31), 293 (40) and 303 (38).

2.3.2. Synthesis of $[Ni(dimethoxybpy)_3](ClO_4)_2$ complex (2)

The complex **2** was prepared using a procedure similar to that for **1** by using dimethoxybpy (3 mmol, 0.65 g) instead of dimethylbpy. The pink product, $[Ni(dimethoxybpy)_3](ClO_4)_2$, was collected by suction filtration, washed with cold water and ether and then air-dried. Yield: 0.6 g, 66%. Anal. Calc. for $C_{36}H_{36}NiN_6Cl_2O_{14}$ (MW = 906.30): C, 47.70; H, 4.00; N, 9.27 %. Found: C, 47.26; H, 3.49; N, 9.79 %. IR (KBr, cm^{-1}): 1611(m) ν(C=N), 1496(m) ν(C=C), and 1096(s) ν(Cl–O); ESI-MS: *m/z* 588.80 $[Ni(dimethoxybpy)_2 + ClO_4]^+$, 534.9 $[Ni(dihydroxybpy)_2 + ClO_4]^+$, 353.0 $[Ni(dimethoxybpy)_3]^{2+}$; UV-visible λ_{max} / nm ($\varepsilon_{max} \times 10^3/M^{-1}\ cm^{-1}$): 233 (67), 285 (23), and 297 (16).

2.3.3. Stability of the complexes in aqueous solution

The kinetic stability of two complexes was evaluated by UV-visible spectral analysis in the Tris /NaCl buffer containing 1% DMSO at 25 °C. The concentration of **1** and **2** was 20 $\times 10^{-6}$ M. Time-dependent stability UV-visible spectra were recorded in the range of 225–320 nm at different times (0, 2, 4, 8, 24, and 48 h).

2.4. X-ray crystallographic procedure

Single crystal X-ray intensity data were collected at ambient temperature (294 K) on a Bruker APEX-II CCD diffractometer equipped with graphite monochromated Mo Kα

radiation (λ = 0.71073 Å) using the *APEX2* program (Bruker, 2008) and processed using the *SAINT* package (Bruker, 2008). Multi-scan absorption correction using the *SADABS* software (Bruker, 2008) was applied to the intensity data. The structure was solved by direct methods using *SHELXT* (Sheldrick, 2015a) and refined with full-matrix least-squares on F^2 on all unique reflections using *SHELX-2014* (Sheldrick, 2015a). All the non-hydrogen atoms were refined anisotropically. The oxygen atoms of a perchlorate anion (Cl2/O3-O6) are disordered over two orientations about a two-fold axis with equal occupancy. During the refimenent of the disordered anion, the O...O distances were constrained to be 2.30(1) Å. The water molecule was also found to be disordered over two sets of sites with a refined occupancy ratio of 0.780(11):0.220(11) for the major and minor components, respectively. An EADP restraint was applied to the displacemnet parameters of the disordered water oxygen atom. The water H atoms were placed in chemically sensible positions on the basis of possible hydrogen bonds with U_{iso}(H) = 1.5U_{eq}(O), but were not refined. All other hydrogen atoms were placed geometrically and refined with isotropic thermal parameters with U_{iso}(H) = 1.2U_{eq}(C) or 1.5U_{eq}(C) for methyl H atoms. A rotation model was used for the methyl groups. Molecular plots were obtained using the *ORTEP-3* (Sheldrick, 2015b) and SCHAKAL-99 (Keller, 1999) programs.

2.5. DNA Binding Experiments

The absorption titrations were performed at room temperature using complexes **1** and **2** at constant concentration of 2.0×10^{-5} M, along with DNA at increasing concentrations of 4.6×10^{-5} to 32×10^{-5} M. UV-visible spectra were recorded in the range of 228–340 nm about 8 min after each addition of DNA solution. The intrinsic binding constant, K_b, was determined using the UV-visible spectra.

In the fluorescence quenching experiments with DNA, the concentration of **1** and **2** was also constant (4×10^{-5} M), against increasing concentrations of DNA ranging from 3×10^{-5} to 27×10^{-5} M. The fluorescence emission spectra were recorded at room temperature and wavelength range of 290–490 nm after exciting the complexes at 270 nm.

Competitive studies of **1** and **2** with GR were investigated by fluorescence spectroscopy in order to examine whether they can displace GR from its DNA-GR system. The emission spectra of GR bound to DNA in the absence and presence of the complexes were recorded for [GR] = 1×10^{-5} M and [DNA] = 1×10^{-4} M, and increasing amounts of the complexes from 4×10^{-6} M to 36×10^{-6} M to reach the [complex]/[GR] ratios ranging from 0.4 to 3.6. Fluorescence emission spectra were recorded in the wavelength range of 540–750 nm after excitation of the GR-DNA system at 520 nm.

For the CD experiments, the concentration of DNA was 10×10^{-5} M and **1** and **2** were 1 and 5×10^{-5} M (r = [complex]/[DNA]= 0.1 and 0.5). The spectra of DNA in the absence and presence of the complexes were recorded in the range of 220–300 nm at room temperature. The solutions were incubated for 10 min after each addition and then its CD spectrum was recorded at 100 nm/min scan rate. The spectrum of Tris buffer was subtracted from sample spectra for data analysis.

2.6. DNA Cleavage Studies

Plasmid DNA of *E. coli* was selected as typical for testing of DNA cleavage ability. Plasmid DNA was purified from a fresh culture with Bio Basic kit. The cleavage of supercoiled pET28a DNA (100 ng/μL) by **1** and **2** in the absence and presence of H_2O_2 (100 μM), as an activating agent, was monitored by gel electrophoresis. Supercoiled pET28a DNA was treated with **1** and **2** and each sample was incubated for 1h at 37 $^{\circ}$C. The samples were then gel electrophoresed at 80 V for 90 min in Tris- Boric acid- EDTA (TBE) buffer using

0.8% agarose gel containing GR. Afterward, the bands were viewed in a Bio Rad Gel doc system and photographed. Densitometric calculations were carried out using the IMAGE J software.

2.7. BSA Binding Experiments

For complex-BSA interactions, the absorption titration experiments were performed at room temperature using a constant concentration of BSA and with increasing concentrations of **1** and **2**. The concentration of BSA was 15×10^{-6} M, and for **1** and **2** spanned from 0 to 45×10^{-5} M. UV-visible spectra were recorded in the range of 250–320 nm. The change in absorbance of the characteristic bands of the BSA at λ_{max} = 280 nm was recorded each time after titrant addition.

In the fluorescence quenching experiments, concentration of BSA was kept fixed at 4×10^{-6} M and concentration of **1** and **2** was varied from 0 to 18×10^{-6} M. The fluorescence emission spectra were recorded at room temperature in the range of 290–450 nm upon excitation at 280 nm.

For SFS also, the same concentrations of BSA and **1** and **2** were used and the spectra were measured at two different $\Delta\lambda$ (difference between the excitation and emission wavelengths of BSA) values of 15 and 60 nm.

For CD experiments, the concentrations of BSA and **1** and **2** were 2 and 10×10^{-6} M, respectively. The CD spectra of BSA in the absence and presence of **1** and **2** were recorded in the range of 200–260 nm at room temperature using a bandwidth of 1 nm, a step interval of 1 nm, an average time of 0.5 s, and a slit width of 0.02 mm. The CD spectrum of Tris buffer was subtracted from the sample spectra for data analysis.

2.8. Theoretical studies

2.8.1. Molecular dynamics simulation

The structure of DNA (PDB ID: 423D) with sequence d(ACCGACGTCGGT)$_2$ and BSA (PDB ID: 4F5S) were taken from the Protein Data Bank (PDB) (http://www.rcsb.org/pdb) with the resolution of 1.60 and 2.47 Å, and the r-value of 0.206 and 0.259 for DNA and BSA, respectively. A 20 ns MD studies were carried out using the GROMACS 4.5.6 (University of Groningen, Netherlands) package (Berendsen, Van der Spoel, & Van Drunen, 1995; Lindahl, Hess, & Van der Spoel, 2001) and the GROMOS96 43a1 force field (Van Gunsteren et al., 1996; Van Gunsteren, Daura, & Mark, 1998). The macromolecules were located in the cubic box with the periodic boundary conditions and the minimum distance between the macromolecules surface and the box was 1.0 nm. The water molecules were added using a simple point charge (SPC216) model and the solvated systems were neutralized by adding Na+ cations (Berendsen, Postma, Van Gunstetren, & Hermans, 1981). Energy minimization was done through using the steepest descent method. Then, the system was equilibrated for 100 ps at the temperature of 300 K. Finally, a 20 ns MD simulation was carried out at 1 bar and 300 K. A Berendsen thermostat (Berendsen, Postma, Van Gunsteren, Di Nola, & Haak, 1984) at 300 K, the particle mesh Ewald (PME) method (Darden, York, & Pedersen, 1993; Essmann et al., 1995) for long range electrostatics, and a 9 Å cut-off for van der Waals and Coulomb interactions were used. The equation of motions was integrated by the leap-frog algorithm with the 2 fs time steps. The atomic coordinates were recorded to the trajectory file every 0.5 ps for later analysis. The stability of simulated systems was scanned using the root-mean-square deviations (RMSDs) of BSA and DNA with respect to their initial structures. The equilibrated conformation of the BSA and DNA were used for docking.

2.8.2. Molecular docking

Docking study was carried out to indicate the active binding site for **1** and **2**. The 3D structure of **1** was generated using the CIF file. The CIF file was converted to the PDB format by using the Mercury software (http://www.ccdc.cam.ac.uk/) and missing hydrogen atoms and Gasteiger charges were added. Flexible-ligand docking was performed by Auto Dock 4.2 molecular-docking program using the implemented empirical free energy function and the Lamarckian Genetic Algorithm (Morris et al., 1998). The Auto Grid was used to calculate grids and a blind docking with 126 lattice points along X, Y, and Z axes was performed to find the active binding sites of the biomacromolecules for **1** and **2**. After determination of the active site, the dimensions of the grid map were selected 60 points with a grid point spacing of 0.375 Å, to allow the ligand to rotate freely. 200 Docking runs with 25,000,000 energy evaluations for each run were performed.

2.9. Cytotoxic activity assays

2.9.1. Cell culture

The cytotoxicity assays were performed using human breast carcinoma cells (MCF-7), human colon carcinoma cells (HT-29), and human brain carcinoma cells (U-87) which were obtained from the cell bank of the Pasteur Institute, Tehran, Iran. These cells were cultured in DMEM and RPMI 1640 medium supplemented with 10% (v/v) heat-inactivated fetal bovine serum (FBS, Gibco), 2 mM of glutamine, and 1% penicillin streptomycin (Invitrogen) in 96 well culture plates, at 37 ^{o}C in a humidified atmosphere in the presence of 5% CO_2.

2.9.2. Cell Viability assay

The cancer cells were seeded at a density of 8×10^3 cells/well into sterile 96 well plates and incubated at 37 ºC in a humidified 5% CO_2 incubator for 24 h. A stock solution of **1** and **2** were prepared in DMSO and diluted with the cell culture medium. The UV-Vis spectral features of **1** and **2** did not change on keeping their DMSO solution for 48 h and no precipitation or turbidity was observed even after longer storage (2 weeks) at room temperature, which indicates the stability of the **1** and **2** in DMSO. After 24 h, the cells were treated in triplicate with increasing concentrations of **1** and **2** (1, 2.5, 5, 10, 20, 40, and 80 μM) and incubated for 24 and 48 h. The MTT colorimetric assay (Mosmann, 1983) was performed to measure the cytotoxic effect of the Ni(II) complexes. At the end of the incubation time, 20 μL of the MTT solution (0.5 mg/mL, Sigma) was added to each well and the cells were incubated again at 37 ºC for 4 h. After 4 h, the medium containing MTT solution was exchanged with 100 μL of DMSO to dissolve the purple formazan crystals formed. The cells were incubated and protected from light for 20 min at room temperature. Then, the cells were shaken for 2 min before reading by multi-mode plate reader (Synergy 2, BioTek, USA) at λ = 570 nm. The absorbance of each well was converted to percentage of cell growth inhibition (Anjomshoa, Torkzadeh-Mahani, Dashtrazmi, & Adeli-Sardou, 2016). The whole experiments were repeated three times for maximum accuracy. The IC_{50} value defined as the drug concentration causing a 50% reduction in cellular viability, was calculated.

3. Results and Discussion

3.1. Syntheses and characterization of the complexes

The tris-chelated complexes $[Ni(NN)_3](ClO_4)_2$, where NN is dimethylbpy (**1)** and dimethoxybpy (**2)**, have been isolated from the aqueous ethanolic solution containing

nickel(II) chloride as the starting material. The complexes **1** and **2** showed good solubility in common polar organic solvents such as CH_3CN, MeOH, DMF, and DMSO. From the elemental analysis results, the desired metal complexes of **1** and **2** were of sufficient purity.

The absorption spectrum of **1** mainly consists of four bands centered at 231, 249, 293, and 303 nm while **2** shows absorption peaks at 233, 285, and 297 nm, which are assigned to the $\pi \rightarrow \pi^*$ electronic transitions of the metal-bound ligands. Both complexes **1** and **2** show three strong bands at 354, 530, and 843 that result from spin-allowed transitions from the ground state ^3A_2g to the excited triplet states $^3T_1g(P)$ $^3T_1g(F)$, and ^3T_2g, respectively. A weak band arises from the spin-forbidden transition to the singlet state ^1Eg, which is observed as a shoulder of the $^3A_2g \rightarrow {}^3T_2g$ transition band at about 850 nm (Supplementary material, Table S1).

As seen in Figs. S1 and S2 in Supplementary material, the IR spectrum of the complexes shows a band at 1617 (**1**) and 1611 (**2**) cm^{-1} due to the stretching frequency for the C=N group and a band at 1486 (**1**) and 1496 (**2**) cm^{-1} due to stretching frequency for the C=C group. The complexes also exhibit the strong absorption band around 1906 cm^{-1} which is assigned to stretching frequency for Cl–O and demonstrates the existence of ClO_4^- as a counter ion.

Formation of metal complexes was confirmed by ESI-MS (Supplementary material, Fig. S3). The spectra of complexes **1** and **2** in MeOH/H_2O show peaks with *m/z* 524.80 and 588.80 corresponding to $[Ni(dimethylbpy)_2 + ClO_4]^+$ and $[Ni(dimethoxybpy)_2 + ClO_4]^+$, respectively. In addition, peaks with *m/z* 305.00 and 353.00 are seen which respectively attribute to $[Ni(dimethylbpy)_3]^{2+}$ and $[Ni(dimethoxybpy)_3]^{2+}$.

3.1.1. Crystal structure of $[Ni(dimethylbpy)_3](ClO_4)_2 \cdot 2H_2O$(1)

X-ray diffraction analysis was only carried out for **1**, the suitable single crystal was obtained by diethyl ether diffusion into a methanol solution of the complex. An ORTEP view of complex **1** is shown in Fig. 1 and the crystallographic data of the complex are summarized in Table 1. Selected bond distances and angles are listed in Table 2. The structure consists of discrete $[Ni(dimethylbpy)_3]^{2+}$ cations, perchlorate anions and water solvent molecules in the stoichiometric molar ratio of 1:2:2. However, one of the two ClO_4^- anions and both water molecules are disordered. Also the complex dication has crystallographically imposed C_2 symmetry, the two-fold axis passing through the metal atom and bisecting one dimethylbpy ligand.

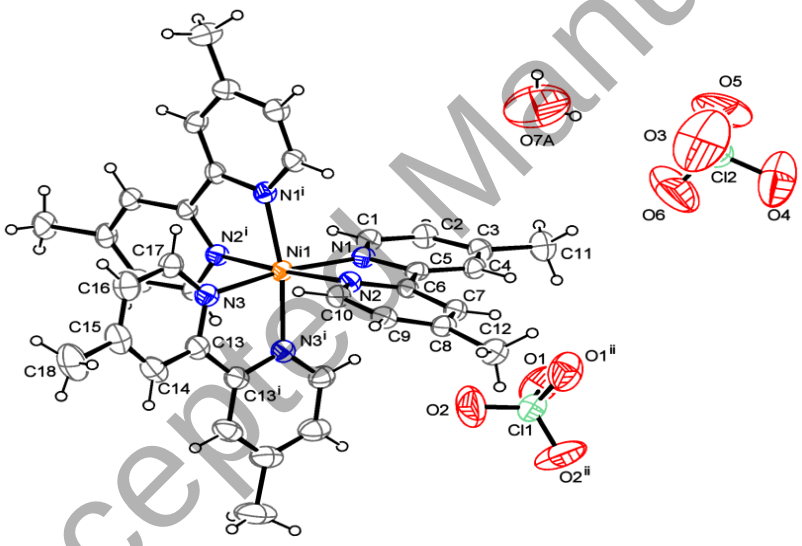

Fig. 1. The asymmetric unit of **1** with displacement ellipsoids drawn at the 30% probability level. One of two perchlorate anions is disordered (with Cl2), and only one orientation of the disordered perchlorate anion is shown. The water molecule is also disordered over two positions and the orientation with the major position is shown. Symmetry codes: (i) 1-x, y. 3/2-z; (ii) 1-x, y, 1/2-z.

Table 1
Crystallographic and data collection parameters for $[Ni(dimethylbpy)_3](ClO_4)_2 \cdot 2H_2O$.

Chemical formul	$C_{36}H_{40}NiN_6Cl_2O_{10}$
Formula weight	846.35
Radiation	Mo K_α (λ = 0.71073 Å)
Temperature (K)	294(2)
Crystal size (mm^3)	0.20 × 0.16 × 0.11
Crystal system	monoclinic
Space group	*C 2/c*
Z	4
a (Å)	11.935(3)
b (Å)	25.886(7)
c (Å)	12.982(4)
β (°)	99.923(4)
Volume ($Å^3$)	3950.8(19)
D_{calc} ($Mg\ m^{-3}$)	1.423
Absorption coefficient (μ) (mm^{-1})	0.689
Absorption correction	multi-scan
$T_{min.}/T_{max.}$	0.548/0.745
Collection ranges	$-14 \le h \le 14$; $-31 \le k \le 31$; $-15 \le l \le 15$
Completeness	99.9 % (θ = 27.00)
Goodness-of-fit on F^2	1.036
Reflections collected / unique	76090 / 4632 [*R(int)* = 0.0352]
Data / restraints / parameters	3683 / 6 / 275
F(000)	1760
θ range for data collection (°)	1.573 - 25.496
Final *R* indices [$I>2\sigma(I)$][a]	*R1* = 0.0627, *wR2* = 0.1564
R indices (all data) [a]	*R1* = 0.1202, *wR2* = 0.2064
Largest difference peak and hole (e $Å^{-3}$)	1.008 and -0.515

[a])$wR=\{\Sigma\ [w(F_o^2-F_c^2)^2]/\Sigma wF_o^4\}^{½}$; $w^{-1}=[\sigma^2(F_o^2) + (0.1075P)^2 + (5.1399P)]$, where $P = (F_o^2 + 2F_c^2)/3$.

Table 2
Selected bond lengths (Å) and bond angles (°) for the complex **1**.

Bond lengths (Å)		*Bond angles* (°)	
Ni—N1	2.069(4)	N1—Ni1—N2	78.60(15)
Ni—N2	2.106(4)	N3—Ni1—N3^{i}	78.8(2)
Ni—N3	2.092(4)	N1—Ni1—N1^{i}	93.1(2)
		N1—Ni1—N2^{i}	98.62(15)
		N1—Ni1—N3	170.74(15)
		N1—Ni1—N3^{i}	94.37(16)
		N2—Ni1—N3	94.87(15)
		N2—Ni1—N3^{i}	88.21(15)
		N2—Ni1—N2^{i}	176.0(2)

Symmetry code: (i) 1-x, y, 3/2-z.

The Ni(II) metal is six-coordinate in a distorted octahedral geometry by the nitrogen atoms of three ligands. The extent of the distortion from the ideal octahedral geometry may be inferred from the values of the N–Ni–N bite angles (78.60(15) and 78.8(2)°) and of the *cis* and *trans* N–Ni–N angles involving different dimethylbpy ligands, ranging respectively from 88.21(15) to 98.62(15)°, and from 170.74(15) to 176.0(2)°. These values, as well as the Ni–N bond lengths (mean value 2.091(11) Å), are in very good agreement with those reported for the strictly related compounds $[Ni(bpy)_3](ClO_4)_2$ (Zhou, Li, Xu, Cao, & Hong, 2003), $[Ni(dimethylbpy)_3](TCNQ)_2$ and $[Ni(dimethylbpy)_3]_2(TCNQ\text{-}TCNQ)(TCNQ)_2\cdot 0.60H_2O$ (Černák et al., 2018), $[Ni(dimethylbpy)_3]I_2\cdot 2H_2O$ (Liu et al., 2014), and $[Ni(dimethylbpy)_3](Sb_3S_5)_2$ (Anderer, Delwa de Alarcón, Näther, & Bensch, 2014).

The pyridine rings of dimethylbpy molecules are not co-planar, but twisted. The twisting angles of N1-C5-C6-N2 and N3-C13-C13^{i}-N3^{i} [(*i*) = 1-x, y, 1.5-z] are -7.2(5)^{o} and 9.7(6)^{o}. Also, the NiC_2N_2 chelate rings adopt a twist conformation, with puckering parameters *q*2 = 0.194(4) Å, φ = 164.7(11)° for Ni1/N1/C5/C6/N2, and *q*2 = 0.072(4) Å, φ = -90(-)° for Ni1/N3/C13/C13^{i}/N3^{i} (symmetry code: (i) 1-x, y, 3/2-z). The dihedral angles between the pyridine rings of the same ligand are 9.23(15)° (N1/C1-C5 ^ N2/C6-C10) and 10.27(18)° (N3/C13-C17 ^ N3^{i}/C13^{i}-C17^{i} ; symmetry code as above).

Figure 2 shows crystal packing of **1** viewed along the *a* axis. The $[Ni(dimethylbpy)_3]^{2+}$ cations related by a *c*-glide plane form layers parallel to (001) plane at z= ¼ and ¾. The ordered ClO_4^- anions also related to a *c*-glide plane are located in the voids between $[Ni(dimethylbpy)_3]^{2+}$ cations above and below the plane at z= ¼ and ¾. The disordered ClO_4^- anions interact with disordered water molecules *via* OH···O (Table 3) forming disordered chains along the [001] direction. The oppositely charged components interact mainly via ionic forces and to a lesser degree via van der Waals forces.

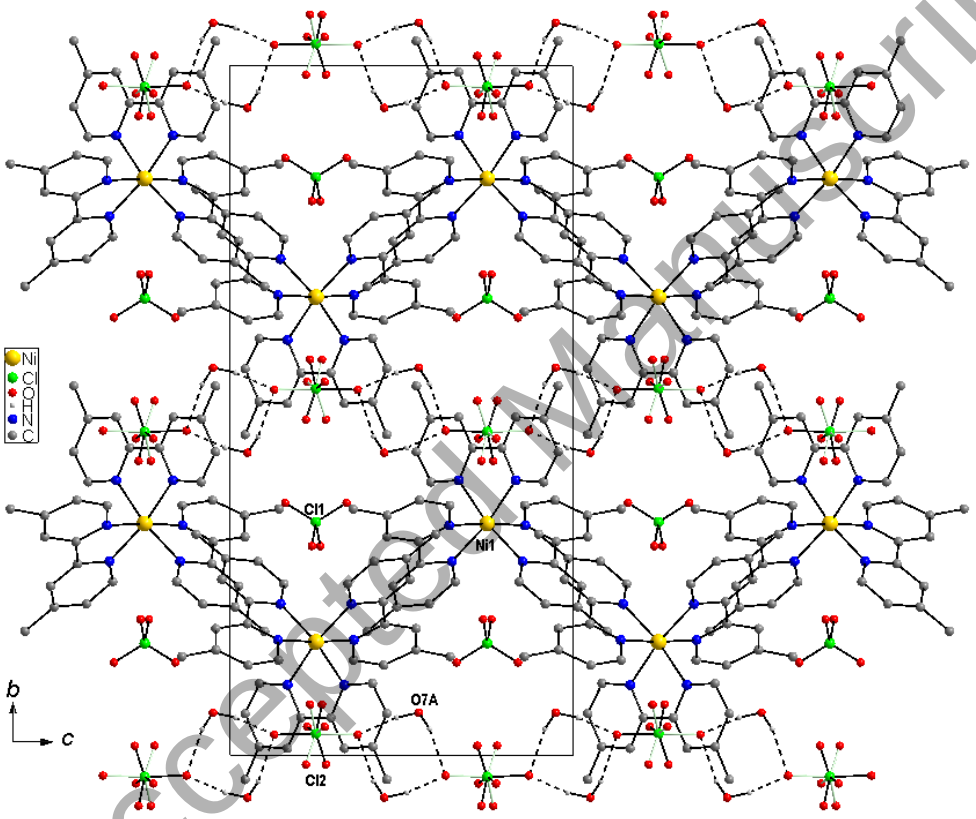

Fig. 2. The crystal packing of **1** viewed along the *a* axis. Hydrogen atoms of dimethylbpy molecules are omitted for clarity. Both orientations of the disordered perchlorate anions (Cl2) are marked in different color (green and black). Only one orientation of the disordered water molecule is shown. Dashed lines represent the OH···O hydrogen bonds linking the disordered ClO_4^- anions.

Table 3
Hydrogen-bonding geometry (Å, °) for the complex **1**.

D—H···*A*	*D*···*A*	H···*A*	*D*—H	*D*—H···*A*
O7A H72 O4i	3.10(3)	2.26	0.86	167
O7A H72 O5ii	3.26(3)	2.49	0.86	149
O7B H74 O3ii	3.08(6)	2.24	0.86	166
O7B H74 O5i	2.99(7)	2.35	0.86	131

Symmetry codes: (i) x, -y, 1/2+z; (ii) 1-x, -y, 1-z.

3.1.2. Stability of the complexes in aqueous solution

Figure S4 indicates the kinetic UV-visible spectra of **1** and **2** at different times in the Tris/NaCl buffer containing 1% DMSO. No drastic absorption changes attributable to instability of the complexes were observed within 48 h, ensuring good stability of these complexes under the test conditions. However, the spectra show slight decrease in absorption with no wavelength shift. This hypochromicity can be attributed to the gradual formation of aggregates of the complexes in solution, which will decrease their effective concentration for UV-visible absorption (Vekshin, 1999).

3.2. DNA Binding Studies

3.2.1. UV-visible Spectral Analysis

It is frequent in the literature that intercalative π-π stacking of the aromatic rings in the metal complexes with the DNA base pairs leads to a reduction and red shift in their absorbance. The extent of the hypochromism and red shift depends on the strength of the interaction between DNA and the complexes (Li, Tian, Gu, Liu, & Yan, 2009; Pyle et al., 1989). The UV-visible absorption was primarily used to address the binding mode of **1** and **2** to DNA. The UV-visible absorption spectra of **1** and **2** in the absence and presence of DNA is displayed in Figs. 3 and 4. The absorbance maxima of 249 and 233 nm respectively for **1** and **2** were found to be more responsive to DNA concentrations and hence were analyzed against

the presence of DNA. As the DNA concentration increased, a clear hypochromic effect was evident reaching 50% for **1** and **2** at the final DNA concentration applied. In addition, a slight red-shift was also observed, suggesting the π-π stacking of **2** with DNA at a moderate degree of binding (Fig.4) (Li, Tian, Gu, Liu, & Yan, 2009; Pyle et al., 1989). Moreover, for a quantitative comparison, the intrinsic binding constant, K_b, was also calculated. The K_b value can be obtained by the ratio of the slope to the intercept in the plot of [DNA] / ($\varepsilon_a - \varepsilon_f$) *vs.* [DNA], according to the following equation (Eq. (1)):

$$[DNA] / \Delta\varepsilon_{ap} = [DNA] / \Delta\varepsilon + 1 / (K_b \times \Delta\varepsilon) \quad (1)$$

in which [DNA] is the concentration of the DNA in base pair, $\Delta\varepsilon_{ap} = |\varepsilon_a - \varepsilon_f|$ (ε_a is the apparent extinction coefficient (A_{obs}/[complex])); $\Delta\varepsilon = |\varepsilon_b - \varepsilon_f|$ (ε_b and ε_f corresponding to the extinction coefficients of the complex in the bound form and free form, respectively). The K_b values for **1** and **2** is 0.1×10^4 M^{-1} (supplementary material, Fig. S5). In the complex **2,** presence of the methoxy-groups can change the orientation of the complex in binding site resulting in conditions provide for formation of π-π stacking interactions with DNA, while the hydrophobic methyl groups are expected to hinder the partial intercalation of the bpy ring in **1**. On the other hand, the hydrophobic interaction of methyl groups with the hydrophobic DNA surface can cause high DNA binding affinity on **1**. Both complexes have the same hypochromic effect (50%) therefore, having the same K_b value can be reasonable. These observed K_b values for the interaction between **1** and **2** with DNA is much smaller than the value obtained for the typical classical intercalator ethidium bromide (EB; $K_b = 4.94 \times 10^5$ M^{-1}) (Ramakrishnan et al., 2011) and smaller than other complexes with N–donar ligands: ($[Ni(dppt)_2Cl_2]$; $K_b = 1 \times 10^4$ M^{-1}) (Anjomshoa, Hadadzadeh, Fatemi, & Torkzadeh-Mahani, 2015), and $[Cu(dimethoxylbpy)_2Cl]PF_6$, $K_b = 0.4 \times 10^4$ M^{-1}) (Anjomshoa et al. 2016), but is similar to the values obtained for other complexes with N–donar ligands:,

[Cu(phen-dione)(bpy)Cl]Cl; $K_b = 0.2 \times 10^4\ M^{-1}$) (Anjomshoa & Torkzadeh-Mahani, 2015), and [Cu(dimethylbpy)$_2$Cl]PF_6, $K_b = 0.1 \times 10^4\ M^{-1}$) (Anjomshoa et al. 2016).

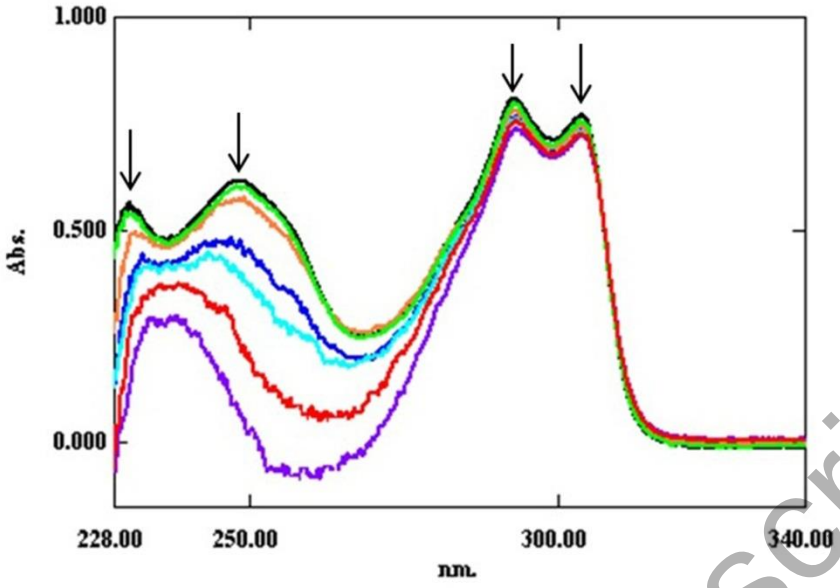

Fig. 3. UV−visible absorption spectra of **1** in the absence and presence of DNA, [complex] = 2.0×10^{-5} M, [DNA] = (0.0, 4.6, 9.2, 13.8, 18.4, 23, 27.6, and 32.0) $\times 10^{-5}$ M. The arrows show the absorbance changes upon increasing amounts of DNA.

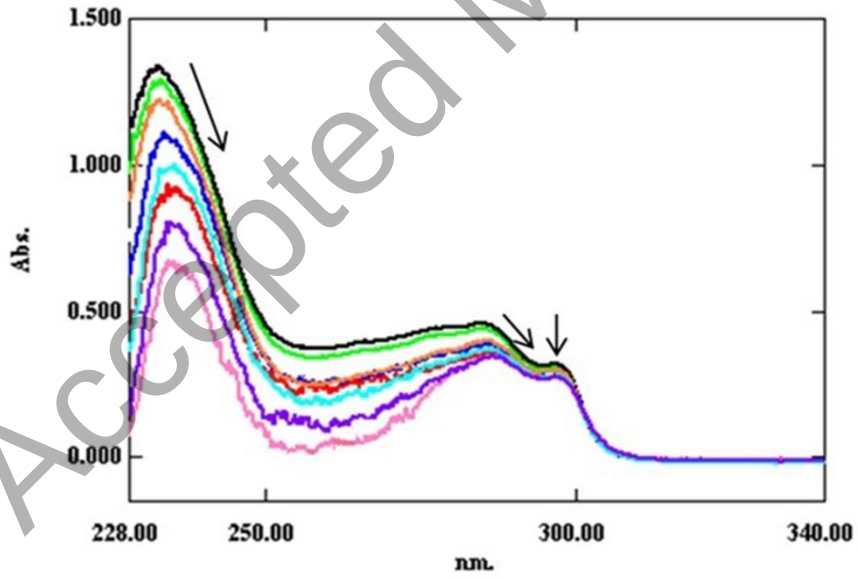

Fig. 4. UV−visible absorption spectra of **2** in the absence and presence of DNA, [complex] = 2.0×10^{-5} M, [DNA] = (0.0, 4.6, 9.2, 13.8, 18.4, 23, 27.6, and 32.0) $\times 10^{-5}$ M. The arrows show the absorbance changes upon increasing amounts of DNA.

3.2.2. Fluorescence Spectral Analysis

The complexes **1** and **2** emitted fluorescence in a Tris buffer, with a maximum wavelength of about 322 nm for **1** and 316 nm for **2** when excited at 270 nm. Figure S6 shows the emission spectra of **1** and **2** in the absence and presence of varying amounts of DNA. Results indicate that DNA could quench the intrinsic fluorescence of **1** and **2**. The quenching provoked by various concentrations of DNA was up to 36% for **1** and 40% for **2**. Also, a new emission at 416 nm grows in intensity, possibly reflecting a change in the complex structure induced in presence of DNA. Indeed, this phenomenon can be used to determine Stern-Volmer constant of the emission intensity quenching of the complexes. The Stern-Volmer constant (K_{SV}) can be calculated from the slope of plot of the emission intensity ratio I_0/I (I_0 and I are respectively the fluorescence intensities in the absence and presence of the quencher) as a function of quencher concentration ([Q]) using the following equation (Eq. (2)) (Lakowicz, 1999):

$$I_0/I = 1 + k_q \tau_0 [Q] = 1 + K_{SV} [Q] \quad (2)$$

Stern-Volmer quenching equation can be used to calculate the values of k_q and K_{SV}. Accordingly, the second-order rate constant for quenching (k_q) is equal to $k_q = K_{SV}/\tau_0$, and τ_0 (the lifetime of the unquenched fluorophore) is typically near 10^{-8} s (Lakowicz & Weber, 1973). Figure S7 indicates plots of I_0/I *vs.* [DNA] that are linear within the experimental concentration range. Table 4 shows the calculated values of K_{SV} and k_q for the interaction of **1** and **2** with DNA. Results of Table 4 reveal that the calculated values of K_{SV} and k_q for **1** and **2** are similar.

Table 4
K_{SV} and kq values for the complex-DNA system.

Complex	K_{SV} ($\times 10^4$ M^{-1})	k_q ($\times 10^{12}$ M^{-1})	R^2
1	0.21	0.21	0.9905
2	0.23	0.23	0.9926

3.2.3. Circular dichroism spectral studies

As previously reported (Kypr, Kejnovska, Renciuk, & Vorlickova, 2009), the CD spectrum of B-form of DNA exhibits a positive band at 277 nm and a negative band at 247 nm, which are assigned to the π-π base stacking of DNA and right-handed DNA helicity, respectively. The observed changes in the CD bands of DNA upon interaction with small molecules may be caused by the induced changes in the secondary structure of DNA. As seen in Fig. 5, at the lower concentrations of **1** and **2**, slight changes is observed in the intensity and position of both positive and negative bands, confirming that the binding mode is non-intercalative mode (electrostatic interaction or groove binding) (Tang, Hou, Mao, & Nian, 2009). At the higher concentrations, however, the two complexes show different effects on DNA structure. The intensity of positive band decreases for the complex **2** which may be a result of partial intercalation of the complex **2** with DNA, while **1** does not seem to cause any alterations.

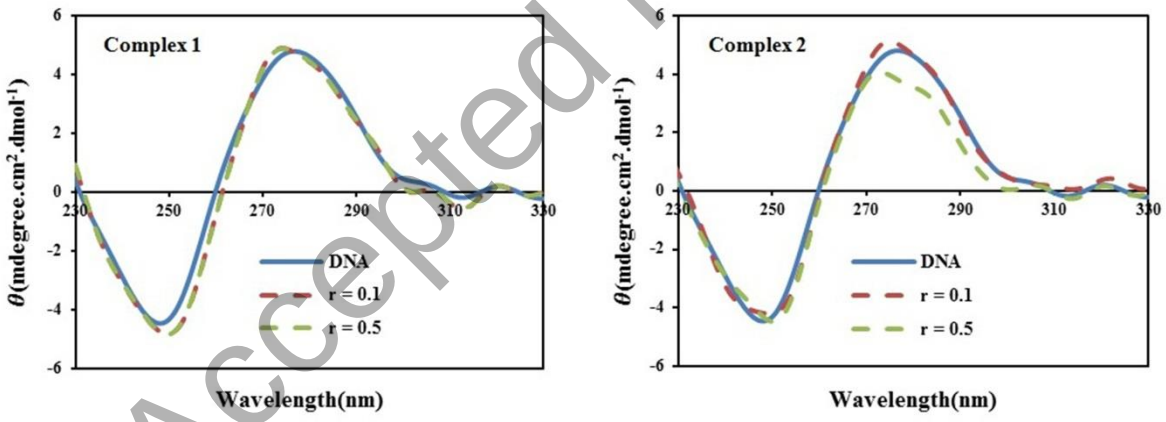

Fig. 5. Circular dichroism spectra of DNA bound by the complexes **1** and **2** with [DNA]/[complex] = 1:0.1 and 1:0.5.

3.2.4. Competitive DNA–binding studies with GelRed

In order to provide further evidence for the mode of interaction between the complexes and DNA, competitive DNA binding with GR as an intercalative probe were performed. Likewise to EB, GR inserts itself between the base pairs in the DNA double helix to form a soluble complex. This in turn results in an increase in GR fluorescence intensity in the presence of DNA with a characteristic emission around 597 nm when excited at 520 nm (Anjomshoa & Torkzadeh-Mahani, 2016). The competitive binding studies involve the addition of **1** and **2** to DNA pre-incubated with GR ([DNA]/[GR] = 10:1) and then the measurement of the emission intensities of GR-DNA system. Figure 6 shows the emission spectra of the GR-DNA solution in the absence and presence of **2**. A small quench in the emission band of the GR-DNA system with the addition of the complex **2** is evident, which indicates that the interaction of complex **2** with DNA is partial intercalation (Anjomshoa & Torkzadeh-Mahani, 2016). The quenching constant (K_{SV}) can be obtained by analyzing the data according to the linear Stern-Volmer (Eq. (2)) (Lakowicz, 1999). The plot of I_0/I *vs.* [complex **2**] is linear (Fig. 6 inset) and K_{SV} value were calculated by the slope of this plot. The K_{SV} value for the complex **2** is 0.6×10^4 M^{-1}. As seen in Fig. S8, no quenching of the emission band of the GR-DNA system with the addition of the complex **1** is observed. This results show the complex **1** cannot compete for DNA-binding sites occupied by GR and its interaction with DNA is external binding type.

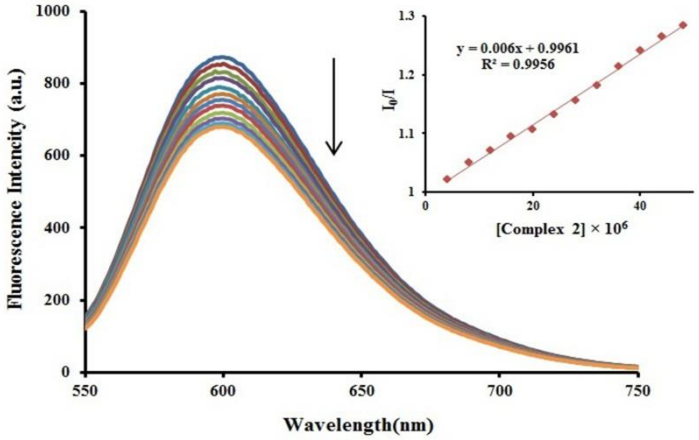

Fig. 6. Emission spectra of GR-DNA in the absence and presence of the complex **2** in Tris /NaCl buffer (pH = 7.2). [Complex]/[GR] = 0.0, 0.4, 0.8, 1.2, 1.6, 2.0, 2.4, 2.8, 3.2 and 3.6. The arrow indicates the emission intensity changes upon increasing the concentration of **2**. Inset: The plot of I_0/I *vs*. [complex 2].

3.3. DNA cleavage studies

The chemical nuclease activity of **1** and **2** was studied by agarose gel electrophoresis experiments with supercoiled pET28a (100 ng/μL) in Tris/ NaCl buffer (pH = 7.2) for 1 h at 37 ºC in the absence and presence of H_2O_2 (100 μM). The plasmid DNA usually exists in three main forms: supercoiled circular (SC, or form I), open circular (OC, or form II) and linear (L, or form III). The cleavage activity is practically conversion of the SC form into OC and/or L forms. The extent of DNA cleavage was estimated from densitometric quantitative results of the gel electrophoresis and diagram thereby obtained (Figs 7 to 10). In the absence of H_2O_2, the complex **1** shows cleavage ability in a concentration-dependent manner so that at the higher concentrations (100 and 120 μM) higher cleavage of SC to both OC and L is observed (Fig. 7, lanes 5 and 6). The conversion of SC DNA into OC form is 33% and 36% and into L form is 26% and 30% at 100 and 120 μM concentrations, respectively. On the other hand, the cleavage ability of **2** is less efficient than **1** (Fig. 8). The cleavage of SC DNA into OC form is 31% and 27% and into L form is 5% and 8% at 100 and 120 μM

concentrations of **2**, respectively. All trials were confirmed by simultaneous control experiments (Figs. 7A and 8A, lane 1).

Further cleavage studies (Figs. 9 and 10) were performed by treating constant concentrations of DNA and H_2O_2 with increasing concentrations of **1** and **2**. As seen in Figs. 9 and 10, both the complexes **1** and **2** show ability of oxidative cleavage of DNA assisted by H_2O_2. The complexes **1** and **2** display cleavage of SC DNA into OC form even at 15 μM concentration (1: 53% and 2: 48%). The cleavage ability of the complexes increases with increasing the concentration of the complexes (Lanes 3–5). Interestingly, it is again the complex **1** exhibits more efficient DNA cleavage activity than **2** most probably because **1** is a groove binder and can cleave plasmid DNA readily (Ramakrishnan, Suresh, Riyasdeen, Akbarsha, & Palaniandavar, 2011) while bipyridine ligand in **2** is supposedly inserted into DNA base pairs. Experimental controls with only H_2O_2 did not show any significant DNA cleavage under similar conditions (data not shown). Generally the oxidative cleavage of DNA involves abstraction of sugar hydrogen by a radical and then the oxidation of deoxyribose or nucleobases. The oxidative cleavage is usually initiated by an external agent like light or H_2O_2. In the presence of H_2O_2, hydroxyl radical species of O_2 (OH) participate in the oxidation of the dexoyribose moiety followed by hydroxyl cleavage of sugar phosphate backbone. (Sangeetha Gowda, Blessy Baby Mathew, Sudhamani, & Bhojya Naik, 2014). In the first step of the oxidative cleavage of DNA by the nickel(II) complexes in the presence of H_2O_2, the putative Ni(III)-oxene/Ni(III)-hydroxo intermediates generate (Rajarajeswari et al., 2013). Then these metal-associated hydroxyl radical species attack to DNA. It is generally accepted that the oxidation mechanism occurs in 3 steps: hydrogen abstraction of deoxyribose, addition of hydroxyl radical to DNA, and electron transfer and resulting in cleavage of DNA backbone. (Kuwabara, Yoon, Goyne, Thederahn, & Sigman, 1986).

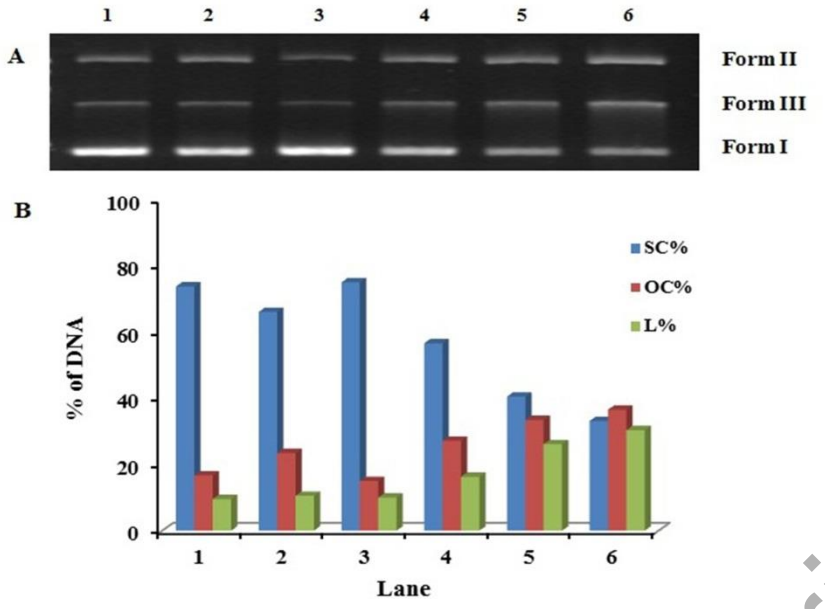

Fig. 7. (A) Gel electrophoresis diagram showing the cleavage of pET28a (100 ng/μL) at different concentrations of **1** in Tris /NaCl buffer (pH 7.2) at 37 ºC for 1 h. Lane 1: DNA alone; Lane 2: DNA + complex **1** (15 μM); Lane 3: DNA + complex **1** (30 μM); Lane 4: DNA + complex **1** (60 μM); Lane 5: DNA + complex **1** (100 μM); Lane 6: DNA + complex **1** (120 μM). **(B)** Densitometric quantitative results of the gel electrophoresis.

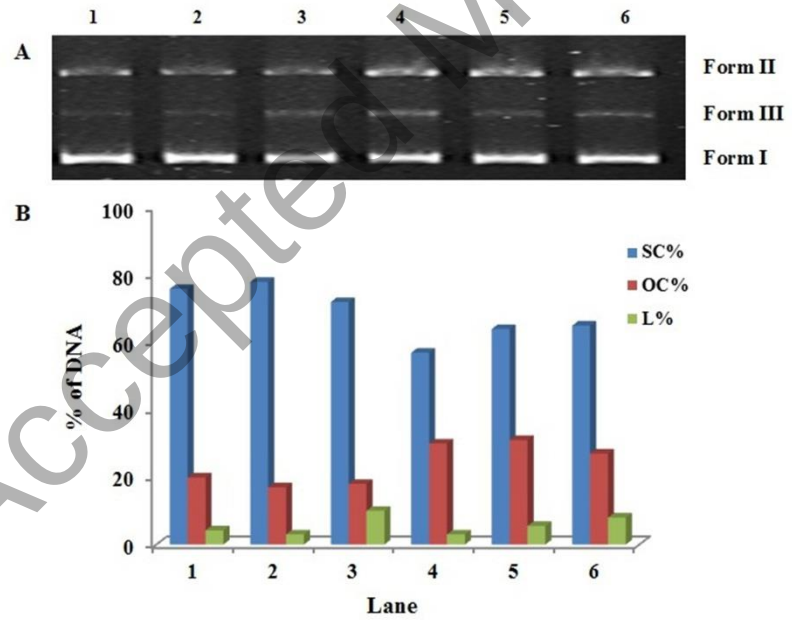

Fig. 8. (A) Gel electrophoresis diagram showing the cleavage of pET28a (100 ng/μL) at different concentrations of **2** in Tris /NaCl buffer (pH 7.2) at 37 ºC for 1 h. Lane 1: DNA alone; Lane 2: DNA + complex **2** (15 μM); Lane 3: DNA + complex **2** (30 μM); Lane 4: DNA + complex **2** (60 μM); Lane 5: DNA + complex **2** (100 μM); Lane 6: DNA + complex **2** (120 μM). **(B)** Densitometric quantitative results of the gel electrophoresis.

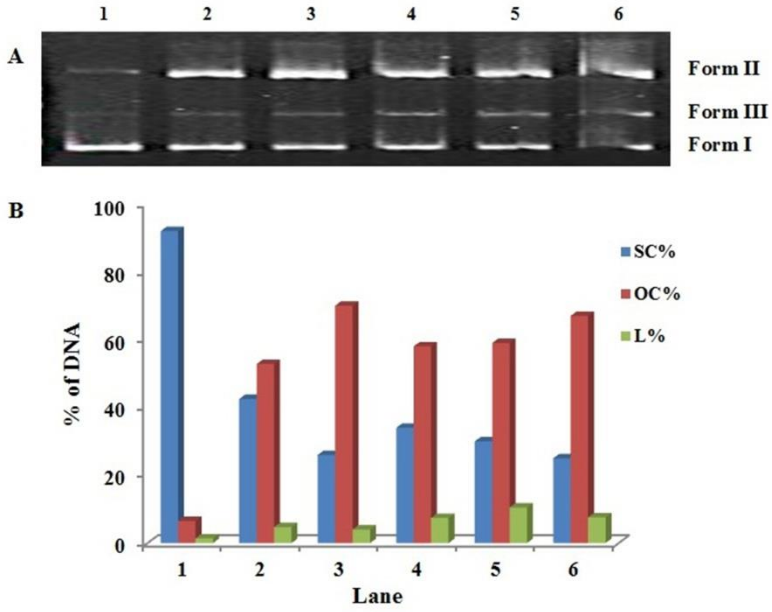

Fig. 9. (A) Gel electrophoresis diagram showing the oxidative cleavage of pET28a (100 ng/μL) at different concentrations of **1** in Tris /NaCl buffer (pH 7.2) at 37 ºC for 1 h in the presence of H_2O_2 (100 μM).. Lane 1: DNA alone; Lane 2: DNA + H_2O_2 + complex **1** (15 μM); Lane 3: DNA + H_2O_2 + complex **1** (30 μM); Lane 4: DNA + H_2O_2 + complex **1** (60 μM); Lane 5: DNA + H_2O_2 + complex **1** (100 μM); Lane 6: DNA + H_2O_2 + complex **1** (120 μM). **(B)** Densitometric quantitative results of the gel electrophoresis.

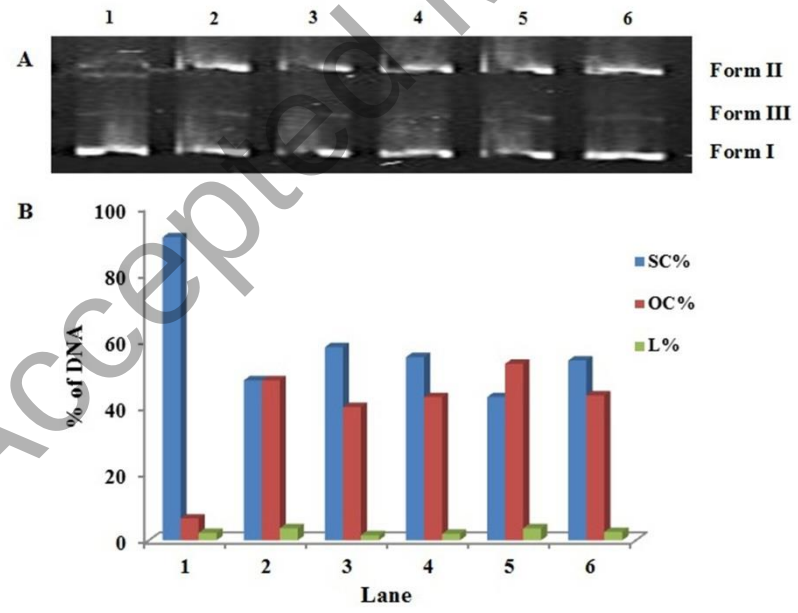

Fig. 10. (A) Gel electrophoresis diagram showing the oxidative cleavage of pET28a (100 ng/μL) at different concentrations of **2** in Tris /NaCl buffer (pH 7.2) at 37 ºC for 1 h in the presence of H_2O_2 (100 μM). Lane 1: DNA alone; Lane 2: DNA + H_2O_2 + complex **2** (15 μM); Lane 3: DNA + H_2O_2 + complex **2** (30 μM); Lane 4:

DNA + H_2O_2 + complex **2** (60 μM); Lane 5: DNA + H_2O_2 + complex **2** (100 μM); Lane 6: DNA + H_2O_2 + complex **2** (120 μM). **(B)** Densitometric quantitative results of the gel electrophoresis.

3.4. BSA Binding Studies

3.4.1. UV-visible Spectral Analysis

UV-visible absorption spectroscopy is used in detecting the conformational changes of proteins and the complex formation. In the present study, to explore the structural changes of BSA by addition of **1** and **2**, we recorded UV-visible spectra of BSA with various amounts of the titled complexes. The weak absorption peak of BSA at 280 nm could be assigned to the polarity of the microenvironment around tyrosine and tryptophan residues of BSA (Polet & Steinhardt, 1968). Figure 11 displays the absorption spectra of BSA in the absence and presence of different amounts of **1** and **2**. It is obvious from Fig. 11 that the characteristic absorption of BSA decreases upon addition of **1** and **2**, and the degree of this intensity decrease is in order of **2** > **1**. These observations indicate the occurrence of the interaction between **1** and **2** with aromatic amino acids of BSA, that may cause the conformational changes in BSA and change the polarity of the microenvironment around the aromatic amino acids of BSA (Alam et al., 2018; Anjomshoa et al., 2015).

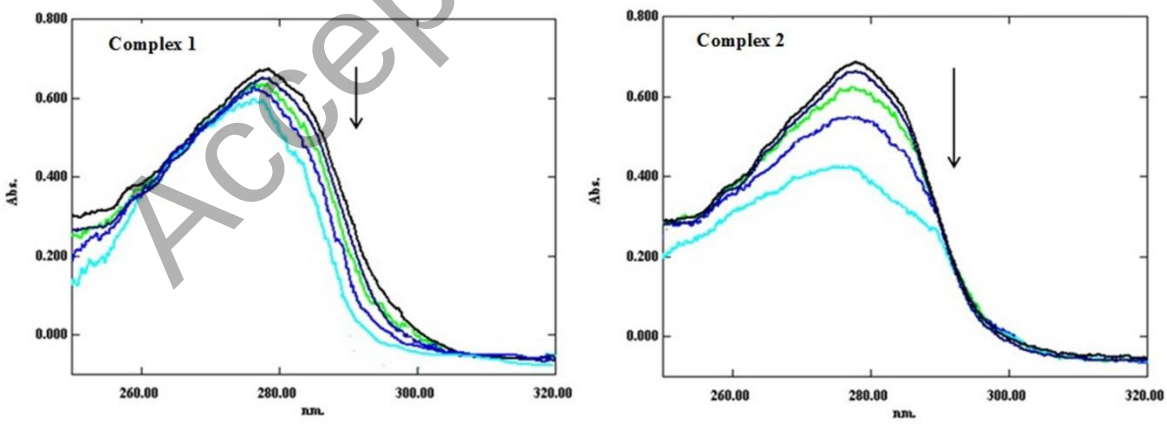

Fig. 11. UV−vis absorption spectra of BSA (15 μM) with increasing concentrations (0–45 μM) of **1** and **2** (Tris /NaCl buffer, pH = 7.2). The arrows show the absorbance changes upon increasing amounts of the complexes.

3.4.2. Fluorescence quenching studies

The effect of **1** and **2** on fluorescence intensity of BSA also was studied. When BSA is titrated with different amounts of **1** and **2**, intrinsic fluorescence decrease of BSA is observed. There are several possible reasons for interpretation the decrease in the emission spectra of BSA, including: the inner filter effect, collisional quenching (dynamic quenching), and binding-related changes in fluorescence (static quenching) (Weert & Stella, 2011). The obtained fluorescence spectra were corrected for the inner filter effects. The following equation (Eq. (3)) can be used to correct the inner filter effects (Pacheco & Bruzzone, 2013):

$$I_{corr} = I_{obs} \text{ antilog } [(A_{ex}+A_{em})/2] \quad (3)$$

Figure 12 shows the corrected emission spectra of BSA in the absence and presence of **1** and **2** at λ_{ex}=280 nm. It should be noted that in conditions of this experiment the emission spectra of the complexes have the lowest intensity (almost zero), which suggests that the effect of the complexes would be negligible. In the corrected emission spectra of BSA in the presence of **1** and **2** the emission intensity of band of BSA decreases (up to 16% of the initial fluorescence intensity for **1** and 34% for **2**). The fluorescence quenching data were analyzed by the Stern–Volmer equation (Eq. (2)) (Lakowicz, 1999), as mentioned before. As shown in Fig. S9, the plots of I_0/I *vs*. [complex] are linear lines. Table 5 shows the calculated values of K_{SV} and k_q.

The binding constants (K_{bin}) can be obtained from the Scatchard model based on that the small molecules are bound to classes of identical and independent binding sites (n), according to the following equation (Eq. (4)) (Scatchard, 1949):

$$\log \frac{I_0-I}{I} = \log K_{bin} + n \log [Q] \quad (4)$$

Figure S9 shows the plots of $\log \frac{I_0-I}{I}$ *vs*. log[Q] and the values of K_{bin} and n (the number of the binding sites on the BSA) can be determined from the intercept and slope of this plots, respectively. Table 5 shows the calculated K_{bin} and n values for interaction of **1** and **2** with

BSA where K_{bin} for **2**-BSA is greater than that of **1**-BSA system at room temperature. The n values for the interaction of **1** and **2** with BSA is found to be equal to 1. This indicates that there is only a single binding site on BSA for these complexes.

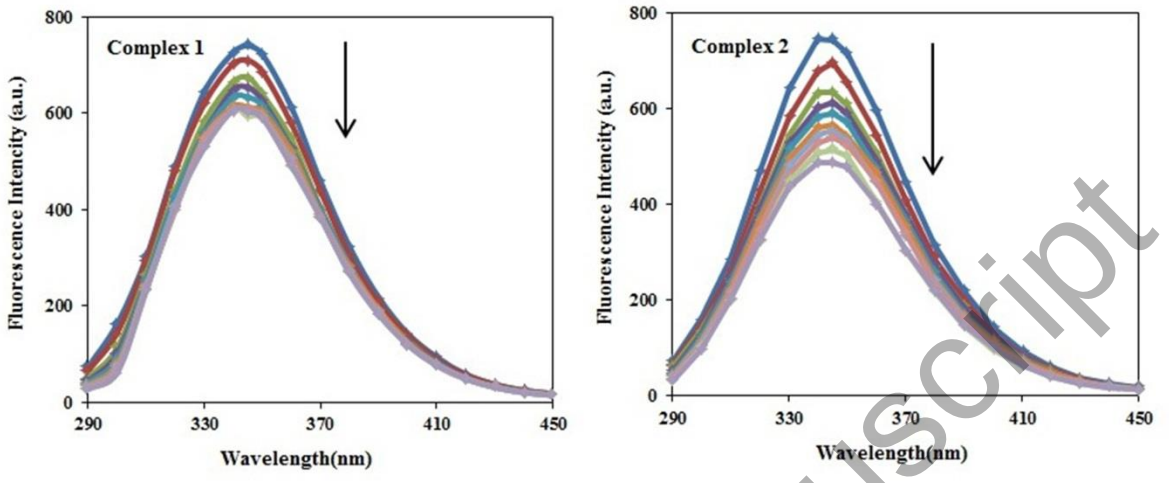

Fig. 12. The corrected emission spectra of BSA (4 μM) in the absence and presence of the complexes **1** and **2** with increasing concentrations (0–18 μM) in Tris/NaCl buffer, pH = 7.2. The arrows show the emission intensity changes upon increasing amounts of the complexes.

Table 5
K_{SV}, kq, K_{bin}, and n values for the complex -BSA system.

Complex	K_{SV} ($\times 10^5$ M^{-1})	k_q ($\times 10^{13}$ $M^{-1}S^{-1}$)	K_{bin} ($\times 10^3 M^{-1}$)	n
1	0.12	0.12	0.55	0.7
2	0.23	0.23	4.3	0.8

3.4.3. Synchronous fluorescence spectra

SFS has become a common tool to investigate conformational changes in proteins due to the presence of other molecules (quenchers). In SFS of BSA, at small $\Delta\lambda$ values ($\Delta\lambda$ = 15), the synchronous fluorescence of a tyrosine-tryptophan mixture is characteristic of tyrosine,

whereas at large Δλ values (Δλ = 60) the spectra is similar to that of tryptophan (Chandel et al., 2018). Figures 13 and 14 show SFS of BSA by increasing the concentration of **1** and **2**. When the concentration of the complexes increased, the SFS intensity of both the tyrosine and tryptophan (Δλ = 15 and Δλ = 60 nm) decrease. As discussed in papers (Ni, Sub, & Kokot, 2010; Qin, Liu, Pan, Fang, & Mou, 2010), SFS can supply characteristic information about the molecular environment in the vicinity of amino acid, such as tyrosine or tryptophan residues, by measuring the possible shift in emission maximum wavelength ($\lambda_{SF,max}$), the shift in position of emission maximum corresponds to the changes of the microenvironment around the amino acid residues. It is apparent from Figs. 13 and 14 that $\lambda_{SF,max}$ of tryptophan (Δλ = 60 nm) shows a blue shif upon the addition of **1** (Fig. 13), which reflects the polarity around the tryptophan decreases and the hydrophobicity increases, whereas $\lambda_{SF,max}$ of tyrosine (Δλ = 15 nm) shows a red shift (Fig. 14) in the presence of **2**, which indicates the environment of tyrosine changes.

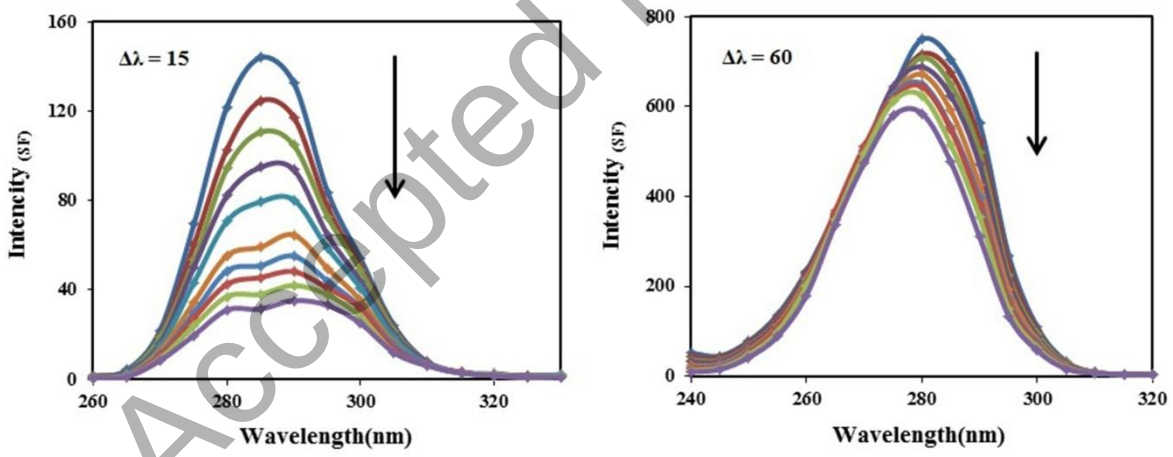

Fig. 13. Synchronous spectra of BSA in the absence and the presence of the complex **1** with increasing concentrations (0–18 μM) in Tris/NaCl buffer, pH = 7.2 at Δλ = 15 and 60 nm. Arrows indicate that the intensity changes upon increasing amounts of the complex.

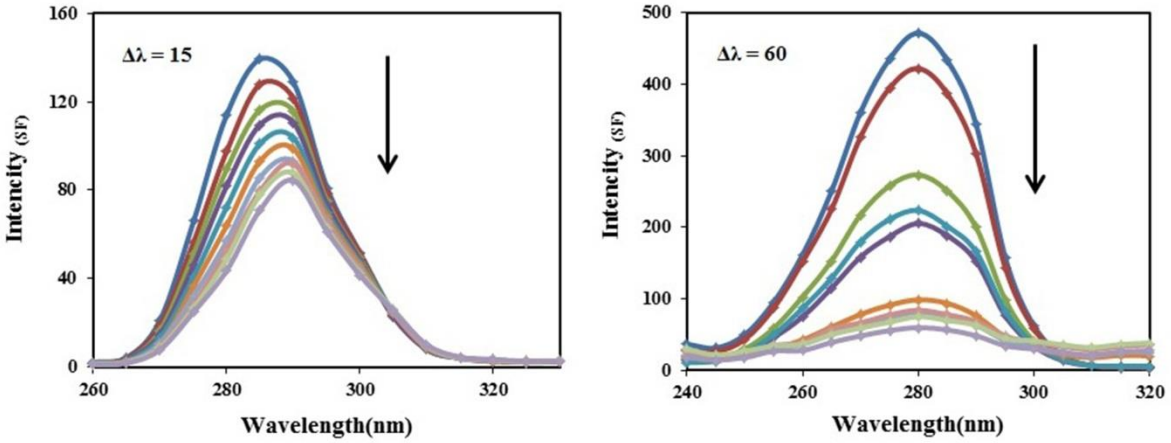

Fig. 14. Synchronous spectra of BSA in the absence and the presence of the complex **2** with increasing concentrations (0–18 μM) in Tris/NaCl buffer, pH = 7.2 at Δλ = 15 and 60 nm. Arrows indicate that the intensity changes upon increasing amounts of the complex.

3.4.4. Circular dichroism spectral studies

Far-UV region of the CD spectrum of BSA gave information on the secondary structure and conformational changes. In this UV region of the CD spectrum, there are two strong negative bands, at 208 nm and 222 nm, which are assigned to the n→π* and π→π* transitions associated with the peptide bond (Nagy et al., 2011). CD spectra of the BSA solution at room temperature recorded in the absence and presence of **1** and **2**. As seen in Fig. 15, both the complexes cause a slight and the same effect on the structure of BSA.

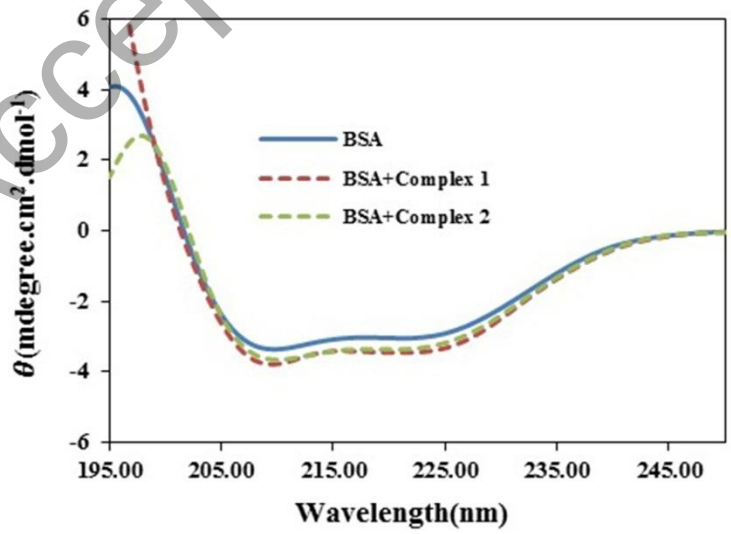

Fig. 15. CD spectra of BSA, [BSA]/[Complex] = 1:1 in Tris buffer at room temperature.

3.5. Molecular docking

3.5.1. Molecular docking of the Ni(II) complexes with DNA sequence d(ACCGACGTCGGT)$_2$

Docking studies were also performed to investigate the DNA binding differences of **1** and **2**. The obtained results from docking of the complexes to DNA sequence d(ACCGACGTCGGT)$_2$ reveal that the Ni(II) complexes fitted into the DNA minor groove (Fig. 16). The binding energy value for the complex **1** is -5.3 and for the complex **2** is -5.7 kcal. mol^{-1}, which reveals that the complex **2** has slightly stronger binding affinity to DNA than the complex **1**. As seen in Table 6, there are hydrophobic contacts between the complex **1** and bases of DNA, including, DT 24, DG 23, DG 22, DG 4, DA 5, and DC 6. While, there are hydrophobic contacts between the complex **2** and bases of DNA, including, DA 17, and DC 9. Interestingly, Ni(II) coordination to the methoxy-substituted bipyridine leads to formation of one hydrogen bonding between the O at 4-postion of bipyridine ring and DG 11 (Fig. 16). Also, the complex **2** is able to form six π-π interactions with bases of DNA (two with DG 16, two with DG 10, one with DG 11, and one with DT 12).Thus, only hydrophobic interactions play significant role in stabilizing of **1** while hydrophobic, hydrogen bonding, and π-π interactions in stabilizing of **2** in minor groove of DNA.

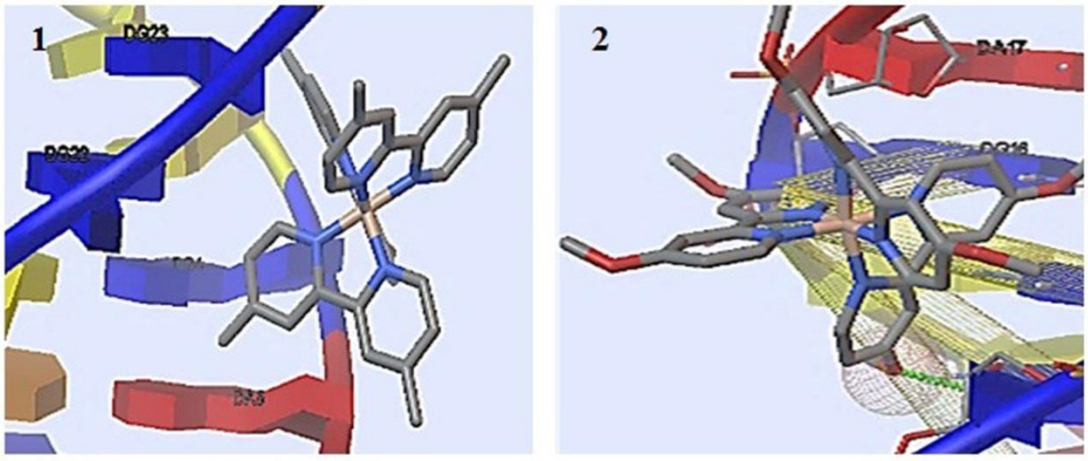

Fig. 16. The docked Ni(II) complexes in the minor groove of DNA sequence d(ACCGACGTCGGT)$_2$, (for the complex **2** H-bond and π-π interactions have been shown as green line and yellow cones, respectively).

Table 6
The results of molecular docking of the complexes **1** and **2** with DNA.

Compound	Binding site	Binding energy of docking (kcal.mol^{-1})	Type of interactions	Adjacent nucleotides within 3 Å distances to complex
1	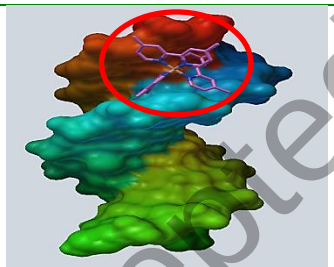	-5.3	Hydrophobic	DT24-DG23 DG22-DG4 DA5-DC6
2	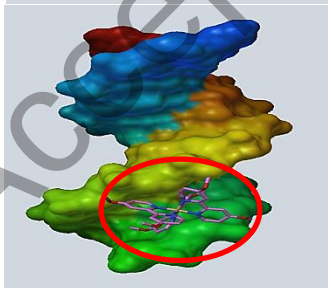	-5.7	Hydrogen bonding, hydrophobic, and π-π interaction	DA17- DG16 DC9-DG10 DG11-DT12

3.5.2. Molecular docking of the Ni(II) complexes with BSA

It has been confirmed that the binding affinity of drugs to serum albumin is the major factor affecting on the distribution and the metabolism of drugs. Therefore the study of interaction between serum albumin and drug is essential to investigate the pharmacokinetics and availability of drugs in tissues. Serum albumin as the most abundant carrier protein comprises three α-helical domains (I, II and III). Table 7 shows the best energy-ranked result of the interaction between the Ni(II) complexes and BSA in all runs of docking procedure. The obtained results from molecular docking show that **1** and **2** have the binding energy of -9.3 and -8.2 kcal.mol^{-1}, respectively (Fig. 17). The complex **1** is nearby to some hydrophobic pockets in domain II of BSA (Glu399, Gly398, Gln403, Arg427, Thr518, Asp517, Tyr400, and Gln521). On the other hand, the complex **2** binds with some hydrophobic pockets in domain II of BSA (Pro 516, Arg 427, Asp 517, Gln 521, Gly 401, Glu 399. Also, there are three hydrogen bonding between the O at 4-postion of bipyridine ring of **2** with some amino acids (Gln 403, Tyr 400, and Thr 518).

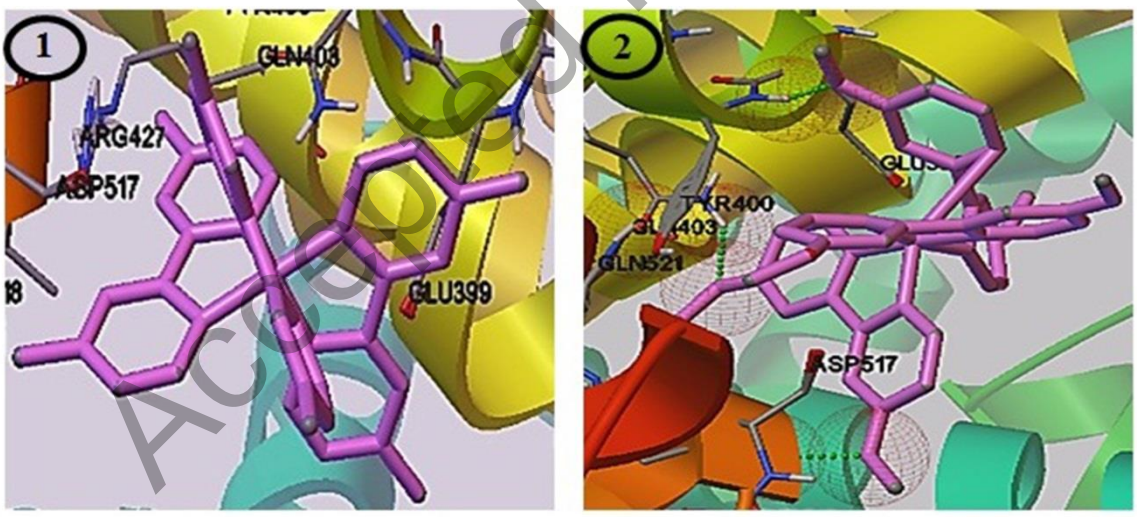

Fig. 17. The docked Ni(II) complexes in the domain I of BSA (for the complex **2** H-bond interactions has been shown as green lines).

Table 7
The results of molecular docking of the complexes **1** and **2** with BSA.

Compound	Binding site	Binding energy of docking (kcal.mol^{-1})	Type of interactions	Adjacent amino acids within 3 Å distances to complex
1	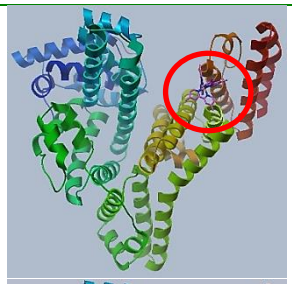	-9.3	Hydrophobic	Glu399-Gly398-Gln403-Arg427-Thr518-Asp517-Tyr400-Gln521
2	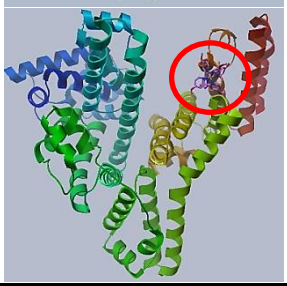	-8.2	Hydrophobic and hydrogen bonding	Pro516-Thr518-Arg427-Asp517-Gln521-Tyr400-Gln403-Gly401-Glu399

3.5. In vitro cytotoxicity studies

The cytotoxicity of **1** and **2** were evaluated against three human cancer cell lines, MCF-7, HT-29, and U-87, in comparison with cisplatin, the most widely used and world's best-selling metal-based anticancer drugs, under identical conditions for both 24 and 48 h incubation time by using MTT assay. Cisplatin was used as a positive control to assess the cytotoxicity of the test compounds. Results reveal that the complexes have no effective cytotoxicity for 24 h incubation time. Table 8 indicates the obtained results for 48 h incubation time. Figure 18 shows plots of percentage of cytotoxicity *vs.* concentrations of **1**, **2**, and cisplatin. According to liturture, the cytotoxicity activities of metal complexes are dependent on their ability to bind with DNA and damage its structure resulting in cell death. Results of DNA binding exhibits although the model of interaction of the Ni(II) complexes is different, but affinity and strength of interactions are the same. The cytotoxicity of the present complexes correlates well with DNA binding affinity. The obtained results show the

similarity in IC_{50} values for **1**, **2** and cisplatin drug in MCF-7 cell line. It is remarkable that **1** is more efficient than **2** in DNA cleavage activity, but the similarity in their cytotoxicity activity obviously due to the similarity in DNA binding affinity. Recent studies indicate that the cytotoxicity activity of tris(diimine)nickel(II) complexes does not necessarily depend on their *in vitro* DNA cleavage abilities (Ramakrishnan et al., 2011). They demonstrated that all the nickel(II) complexes, in spite of their inability to cleave DNA, exhibit high cytotoxic properties, which correlates well with their high DNA binding affinity. Also, the ability of Ni(II) 5,6-dmp complexes to exhibit cytotoxicity and DNA binding affinity higher than the phen analogue is in line with the hydrophobic interactions of methyl groups on 5,6-dmp ligand .

Table 8
The obtained IC_{50} values (μM) for the complexes in 48 h incubation time against human cell lines. The results are expressed as the mean ± SD (n = 3).

Compound	MCF-7	HT-29	U-87
1	37±1.4	36±3.2	39±2.2
2	40±2.1	37±2.8	24±0.9
cisplatin	36±4.6	23±1.8	27±1.5

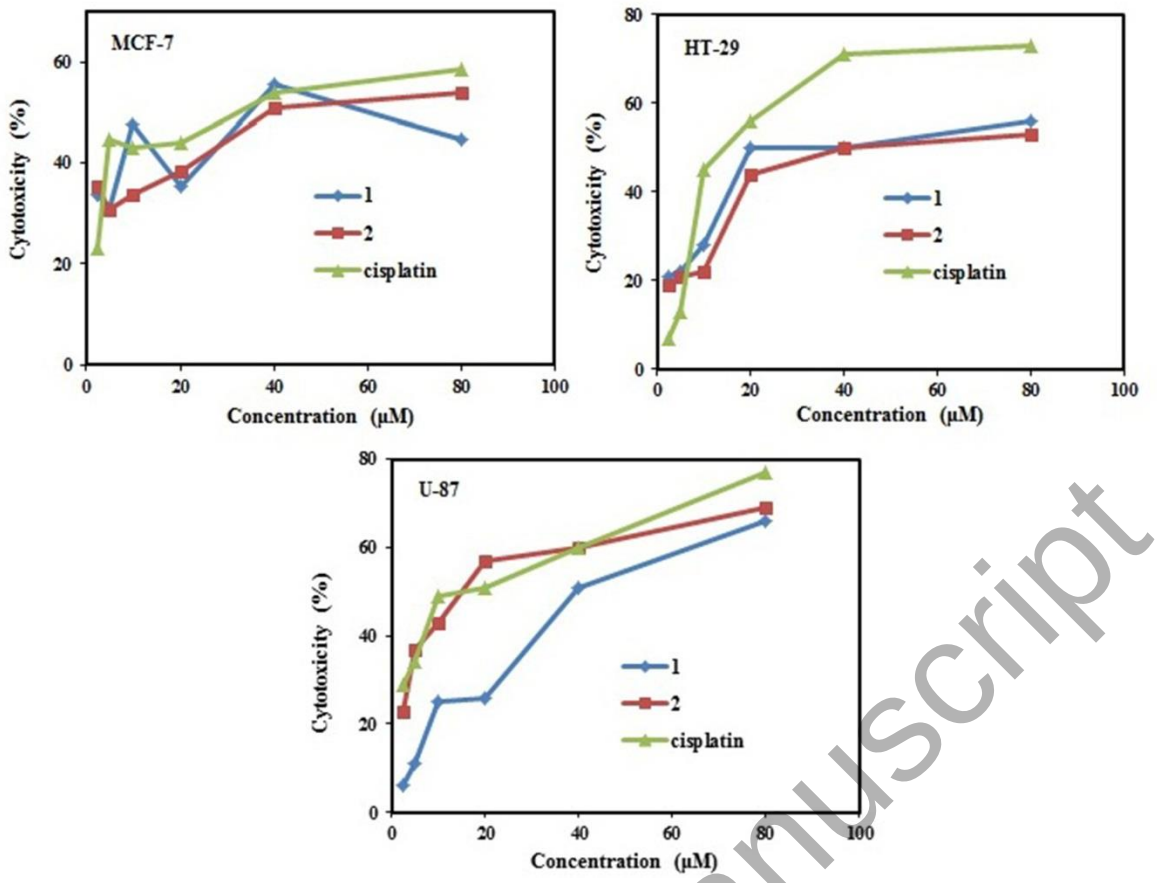

Fig. 18. Plots of percentage of cytotoxicity *vs.* concentration of **1**, **2**, and cisplatin against the MCF-7, HT-29, and U-87 cell lines.

4. Conclusion

The main purpose of this research was to study of the structure–activity relationship of the two nickel(II) complexes with substituted bipyridine ligands, $[Ni(dimethylbpy)_3](ClO_4)_2$ (**1**) and $[Ni(dimethoxybpy)_3]$ $(ClO_4)_2$ (**2**). Characterization of the complexes was done by FT-IR, CHN, and ESI-MS techniques and also by single-crystal X-ray crystallography for the complex **1**. X-ray crystal structure of this complex shows Ni(II) located in a distorted octahedral geometry. The interaction between the complexes and DNA was investigated using techniques such as absorption, emission, CD, and a relative DNA binding study with GR. The outcomes of physicochemical measurements suggest that **1** and **2** interact with DNA

via groove and partial intercalative binding modes, respectively. The complexes only differ in substitutions on their ligand being either a methyl- or a methoxy-group, to which their difference in interaction toward DNA can be correlated. In addition, methyl-substituted bipyridine were found to be ineffective for intercalative binding with DNA. Molecular docking results show that only hydrophobic interactions play a significant role in stabilizing **1,** while there are hydrophobic, hydrogen bonding, and π-π interactions between **2** and DNA in minor grooves. We accordingly propose that hydrogen-bonding and π-π interactions, which occur between ligand in the complex **2** with DNA, would contribute significantly to the partial intercalative binding of **2**. The complex **1** displays more effective DNA cleavage in the absence and presence of H_2O_2 than **2** and hence is a better chemical nuclease. Moreover, the ability of complexes to bind to BSA was also investigated by UV-visible, emission and synchronous fluorescence, and CD in order to show if BSA can act as biological target for our compounds. Results of experimental and molecular modeling confirm that **1** and **2** interact with the hydrophobic domains of BSA *via* noncoordinate interactions. The binding force of **1** to BSA is hydrophobic, whereas **2** docks to BSA *via* hydrophobic and hydrogen-bonding interactions. The cytotoxicity of the present complexes correlates with their DNA binding affinity and not their DNA cleavage activity. The obtained results show the similarity in their cytotoxicity activity obviously due to the similarity in DNA binding affinity.

Acknowledgments

Authors would like to thank the head of Pharmaceutics Research Center, Institute of Neuropharmacology, and Vice-chancellor for Research, Kerman University of Medical Sciences for their financial support of this project (Research proposal no. 95000234).

Appendix A. Supplementary material

CCDC 1433225 contains the supplementary crystallographic data for **1**. These data can be obtained free of charge via http://www.ccdc.cam.ac.uk/conts/retrieving.html, or from the Cambridge Crystallographic Data Centre, 12 Union Road, Cambridge CB2 1EZ, UK; fax: +44 1223 336 033; or e-mail: deposit@ccdc.cam.ac.uk. Supplementary data associated with this article can be found in the online version.

References

Alam, M. M., Qais, F. A., Ahmad, I., Alam, P., Khan, R. H., & Naseem, I. (2018). Multi-spectroscopic and molecular modelling approach to investigate the interaction of riboflavin with human serum albumin. *Journal of Biomolecular Structure and Dynamics, 36*, 795–809.

Alomar, K., Landreau, A., Allain, M., Bouet, G., & Larcher G. (2013). Synthesis, structure and antifungal activity of thiophene-2,3-dicarboxaldehyde bis(thiosemicarbazone) and nickel(II), copper(II) and cadmium(II) complexes: Unsymmetrical coordination mode of nickel complex. *Journal of Inorganic Biochemistry, 126*, 76–83.

Anderer, C., Delwa de Alarcón, N., Näther, C., & Bensch, W. (2014). A strategy for the preparation of thioantimonates based on the concept of weak acids and corresponding strong bases. *Chemistry A European Journal, 20*, 16953–16959.

Anjomshoa, M., Hadadzadeh, H., Fatemi, S. J., & Torkzadeh-Mahani, M. (2015). A mononuclear Ni(II) complex with 5,6-diphenyl-3-(2-pyridyl)-1,2,4-triazine: DNA- and BSA-binding and anticancer activity against human breast carcinoma cells. *Spectrochimica Acta Part A, 136*, 205–215.

Anjomshoa, M., Hadadzadeh, H., Torkzadeh-Mahani, M., Fatemi, S. J., Adeli-Sardou, M., Amiri Rudbari, H., & Nardo, V.M. (2015). A mononuclear Cu(II) complex with 5,6-diphenyl-3-(2-pyridyl)-1,2,4-triazine: Synthesis, crystal structure, DNA- and BSA-binding, molecular modeling, and anticancer activity against MCF-7, A-549, and HT-29 cell lines. *European Journal of Medicinal Chemistry, 96*, 66–82.

Anjomshoa, M., & Torkzadeh-Mahani, M. (2015). *In vitro* DNA and BSA-binding, cell imaging and anticancer activity against human carcinoma cell lines of mixed ligand copper(II) complexes. *Spectrochimica Acta Part A,150*, 390–402.

Anjomshoa, M., & Torkzadeh-Mahani, M. (2016). Competitive DNA-binding studies between metal complexes and GelRed as a new and safe fluorescent DNA dye. *Journal of Fluorescence, 26*, 1505–1510.

Anjomshoa, M., Torkzadeh-Mahani, M., Dashtrazmi, E., Adeli-Sardou, M. (2016). Sonochemical synthesis and characterization of the copper(II) nanocomplex: DNA- and BSA-binding, cell imaging, and cytotoxicity against the human carcinoma cell lines. *Journal of Fluorescence, 26*, 545–558.

Anjomshoa, M., Torkzadeh-Mahani, M., Janczak, J., Rizzoli, C., Sahihi, M., Ataei, F., & Dehkhodaei, M. (2016). Synthesis, crystal structure and Hirshfeld surface analysis of copper(II) complexes: DNA- and BSA- binding, molecular modeling, cell imaging and cytotoxicity. *Polyhedron, 119*, 23–38.

Arounaguiri, S., & Maiya, B. G. (1996). Dipyridophenazine complexes of cobalt(III) and nickel(II): DNA-binding and photocleavage studies. *Inorganic Chemistry, 35*, 4267–4270.

Berendsen, H. J. C., Postma, J. P. M., Van Gunstetren, W. F., & Hermans, J. (1981). *Intermolecular Forces, B.* Pullman (Ed.), Reidel, Dordrecht, The Netherlands.

Berendsen, H. J. C., Postma, J. P. M., Van Gunsteren W. F., Di Nola, A., & Haak, J.R. (1984). Molecular dynamics with coupling to an external bath. *The Journal of Chemical Physics, 81*, 3684–3690.

Berendsen, H. J. C., Van der Spoel, D., & Van Drunen, R. (1995). GROMACS: A message-passing parallel molecular dynamics implementation. *Computer Physics Communications, 91*, 43–56.

Bruker, APEX2, SAINT and SADABS, Bruker AXS Inc. (2008). Madison, Wisconsin, USA.

Černák, J., Hegedüs, M., Váhovská, L., Kuchár, J., Šoltésová, D., Čižmár, E.,… & Falvello, L.R. (2018). Syntheses, crystal structures and magnetic properties of complexes based on $[Ni(L\text{-}L)_3]^{2+}$ complex cations with dimethyl derivatives of 2,2'-bipyridine and TCNQ. *Solid State Sciences, 77*, 27–36.

Chandel, T. I., Rabbani, G., Vahid Khan, M., Zaman, M., Alam, P., Shahein, Y., & Hasan Khan, R. (2018). Binding of anti-cardiovascular drug to serum albumin: An insight in the light of spectroscopic and computational approaches, *Journal of Biomolecular Structure and Dynamics, 36*, 54–67.

Darden, T., York, D., & Pedersen, L. (1993). Particle mesh Ewald: An $N\cdot\log(N)$ method for Ewald sums in large systems. *The Journal of Chemical Physics, 98*, 10089–10092.

Essmann, U., Perera, L., Berkowitz, M. L., Darden, T., Lee, H., & Pedersen, L. G. (1995). A smooth particle mesh Ewald method. *The Journal of Chemical Physics, 103*, 8577–8593.

Gao, C., Ma, Z., Zhang, Y., Li, S., Gu, W., Liu, X., … & Yan. S. (2015). Four related mixed-ligand nickel(II) complexes: Effect of steric encumbrance on the structure, DNA/BSA binding, DNA cleavage and cytotoxicity. *RSC Advances, 5*, 30768–30779.

Keller, E. (1999). *SCHAKAL99*. University of Freiberg, Germany.

Kosiha, A., Parthiban, C., Ciattini, S., Chelazzi, L., & Elango, K. P. (2017). Metal complexes of naphthoquinone based ligand: Synthesis, characterization, protein binding, DNA

binding/cleavage and cytotoxicity studies, *Journal of Biomolecular Structure and Dynamics*. Advance online application. DOI: 10.1080/07391102.2017.1413423.

Kuwabara, M., Yoon, C., Goyne, T., Thederahn, T., & Sigman, D. *S.* (1986). Nuclease activity of 1,l0-phenanthroline-copper ion: Reaction with CGCGAATTCGCG and its complexes with Netropsin and *Eco*RI. *Biochemistry*, *25*, 7401–7408.

Kypr, J., Kejnovska, I., Renciuk, D., & Vorlickova, M. (2009). Circular dichroism and conformational polymorphism of DNA. *Nucleic Acids Research, 37*, 1713–1725.

Lakowicz, J. R., & Weber, G. (1973). Quenching of fluorescence by oxygen. Probe for structural fluctuations in macromolecules. *Biochemistry, 12*, 4161–4170.

Lakowicz, J. R. (1999). *Principles of Fluorescence Spectroscopy*. Plenum Press: New York.

Li, D. D., Tian, J. L., Gu, W., Liu, X., & Yan, S. P. (2009, October). Synthesis, X-ray crystal structures, DNA binding and nuclease activities of two novel 1,2,4-triazole-based Cu^{II} complexes. *European Journal of Inorganic Chemistry*, 5036–5045.

Lindahl, E., Hess, B., & Van der Spoel, D. (2001). GROMACS 3.0: a package for molecular simulation and trajectory analysis. *Molecular Modeling Annual, 7*, 306–317.

Liu, H. X., Xu, Y., Li, F., Guo, H. M., Ye, K. Q., Wang, L. T., & Cao, H. (2014). Study on a structure of Tris-(4,4'-dimethyl-2,2'-dipyridyl)-Ni iodine hydrate, $Ni(C_{12}H_{12}N_2)_3 \cdot 2I \cdot H_2O$. *Journal of Chemical and Pharmaceutical Research, 6*, 1373-1376.

Marmur, J. (1961). A procedure for the isolation of deoxyribonucleic acid from micro–rganisms. *Journal of Molecular Biology, 3*, 208–218.

Maroney, M. J. (1999). Structure/function relationships in nickel metallobiochemistry. *Current Opinion in Chemical Biology, 3*, 188–l99.

Meng, X. Y., Zhang, H. X., Mezei, M., & Cui, M. (2011). Molecular Docking: A powerful approach for structure-based drug discovery. *Current Computer–Aided Drug Design,7*, 146–157.

Morris, G. M., Goodsell, D. S., Halliday, R. S., Huey, R., Hart, W. E., Belew, R. K., & Olson, A. J. (1998). Automated docking using a Lamarckian genetic algorithm and an empirical binding free energy function. *Journal of Computional Chemistry, 19*, 1639–1662.

Morshedi, M., & Hadadzadeh, H. (2013). Mononuclear Co(III) and Ni(II) complexes with polypyridyl ligands, $[Co(phen)_2(taptp)]^{3+}$ and $[Ni(phen)_2(taptp)]^{2+}$: Synthesis, photocleavage and DNA-binding. *Journal of Fluorescence, 23*, 259–264.

Mosmann, T. J. (1983). Rapid colorimetric assay for cellular growth and survival: Application to proliferation and cytotoxicity assays. *Journal of lmmunological Methods, 65*, 55–63.

Nagy, E. M., Nardon, C., Giovagnini, L., Marchio, L., Trevisan, A., & Fregona, D. (2011). Promising anticancer mono- and dinuclear ruthenium(III) dithiocarbamato complexes: systematic solution studies. *Dalton Transactions, 40*, 11885–11895.

Ni, Y., Su, S., & Kokot, S. (2010). Spectrometric studies on the interaction of fluoroquinolones and bovine serum albumin. *Spectrochimica Acta Part A, 75*, 547–552.

Pacheco, M. E., & Bruzzone, L. (2013). Synchronous fluorescence spectrometry: Conformational investigation or inner filter effect?. *Journal of Luminescence, 137*, 138–142.

Palchaudhuri, R., & Hergenrother, P. J. (2007). DNA as a target for anticancer compounds: methods to determine the mode of binding and the mechanism of action. *Current Opinion in Biotechnology, 18*, 497–503.

Patra, A., Sen, B., Sarkar, S., Pandey, A., Zangrando, E., & Chattopadhyay, P. (2013). Nickel(II) complexes with 2-(pyridin-3-ylmethylsulfanyl)phenylamine and halide/pseudohalides: Synthesis, structural characterisation, interaction with CT-DNA and bovine serum albumin, and antibacterial activity. *Polyhedron, 51*, 156–163.

Polet, H., & Steinhardt, J. (1968). Binding-induced alterations in ultraviolet absorption of native serum albumin. *Biochemistry, 7*, 1348–1356.

Pyle, A. M., Rehmann, J. P., Meshoyrer, R., Kumar C. V., Turro, N. J., & Barton, J. K. (1989). Mixed-ligand complexes of ruthenium (II): Factors governing binding to DNA. *Journal of the American Chemical Society, 111*, 3051–3058.

Qin, P., Liu, R., Pan, X., Fang, X., & Mou, Y. (2010). Impact of carbon chain length on binding of perfluoroalkyl acids to bovine serum albumin determined by spectroscopic methods. *Journal of Agricultural and Food Chemistry, 58*, 5561–5567.

Rajarajeswari, C., Loganathan, R., Palaniandavar, M., Suresh, E., Riyasdeend, A., Akbarshae, M. A. (2013). Copper(II) complexes with 2NO and 3N donor ligands: synthesis, structures and chemical nuclease and anticancer activities. *Dalton Transactions, 42*, 8347–8363.

Ramakrishnan, S., Shakthipriya, D., Suresh, E., Periasamy, V. S., Abdulkader Akbarsha, M., & Palaniandavar, M. (2011). Ternary dinuclear copper(II) complexes of a hydroxybenzamide ligand with diimine coligands: the 5,6-dmp ligand enhances DNA binding and cleavage and induces apoptosis. *Inorganic Chemistry, 50*, 6458–6471.

Ramakrishnan, S., Suresh, E., Riyasdeen, A., Akbarsha, M. A., & Palaniandavar, M. (2011). Interaction of *rac*-$[M(diimine)_3]^{2+}$ (M = Co, Ni) complexes with CT DNA: role of 5,6-dmp ligand on DNA binding and cleavage and cytotoxicity. *Dalton Transactions, 40*, 3245–3256.

Raman, N., Pothiraj, K., & Baskaran, T. (2011). DNA interaction, antimicrobial, electrochemical and spectroscopic studies of metal(II) complexes with tridentate heterocyclic Schiff base derived from 2'-methylacetoacetanilide. *Journal of Molecular Structure, 1000*, 135–144.

Rijt, S. V., & Sadler, P. J. (2009). Current applications and future potential for bioinorganic chemistry in the development of anticancer drugs. *Drug Discovery Today, 14*, 1089–1097.

Rosenberg, B., Van Camp, L., Trosko, J. E., & Mansour, V. H. (1969). Platinum compounds: a new class of potent antitumour agents. *Nature, 222*, 385–386.

Sangeetha Gowda, K.R., Blessy Baby Mathew, Sudhamani, C. N., & Bhojya Naik, H. S. (2014). Mechanism of DNA binding and cleavage. *Biomedicine and Biotechnology, 2, 1–9.*

Scatchard, G. (1949). The Attractions of proteins for small molecules and ions. *Annals of the New York Academy of Sciences*, *51*, 660–672.

Sheldrick, G. M. (2015a). *SHELXT* - Integrated space-group and crystal-structure determination. *Acta Crystallographica Section A, 71*, 3–8.

Sheldrick, G. M. (2015b). Crystal structure refinement with *SHELXL*. *Acta Crystallographica Section C, 71*, 3–8.

Tabrizi, L., Talaie, F., & Chiniforoshan, H. (2016). Copper(II), cobalt(II) and nickel(II) complexes of lapachol: Synthesis, DNA interaction and cytotoxicity. *Journal of Biomolecular Structure and Dynamics*, *35*, 3330–3341.

Tang, S. P., Hou, L., Mao, Z. W., & Nian, L. (2009). Synthesis, crystal structures, DNA binding and oxidative cleavage studies of copper(II) complexes of N_2S_2 tetradentate ligands. *Polyhedron, 28*, 586–592.

Topală, T., Bodoki, A., Oprean, L., & Oprean, R. (2014). Bovine serum albumin interactions with metal complexes. *Clujul Medical, 87*, 215–219.

Van Gunsteren, W. F., Billeter, S. R., Eising, A. A., Hünenberger, P.H., Krüger, P. K. H. C., Mark, A. E., … & Tironi, I. G. (1996). *Biomolecular Simulation: The GROMOS96 Manual and User Guide*. Vdf Hochschulverlag AG, Zürich.

Van Gunsteren, W. F., Daura, X., Mark, A. E. (1998). *Encyclopedia of Computational Chemistry*. P. Von Rague Schleyer, Chichester, UK Wiley and Sons.

Vekshin, N. L. (1999). Screening hypochromism in molecular aggregates and biopolymers. *Journal of Biological Physics*, *25*, 339–354.

Vinuelas-Zahinos, E., Luna-Giles, F., Torres-Garcia, P., & Fernandez-Calderon, M. C. (2011). Co(III), Ni(II), Zn(II) and Cd(II) complexes with 2-acetyl-2-thiazoline thiosemicarbazone: Synthesis, characterization, X-ray structures and antibacterial activity. *European Journal of Medicinal Chemistry*, *46*, 150–159.

Weert, M., & Stella, L. (2011). Fluorescence quenching and ligand binding: A critical discussion of a popular methodology. *Journal of Molecular Structure*, *998*, 144–150.

Zhou, Y., Li, X., Xu, Y., Cao, R., & Hong, M. (2003). Tris(2,2'-bipyridine)nickel(II) diperchlorate. *Acta Crystallographica Section E*, *59*, 300–303.